# Tight binding method (CO-LCBO)

Only the interaction with the nearest neighbours are taken into account: only the exchange integral β with the nearest neighbour (*E*~α, *t*~β,*S*<<1)

$$H(\vec{k}) = \alpha + \beta e^{ik_x a} + \beta e^{-ik_x a} = \alpha + 2\beta \cos k_x a$$

$$H(\vec{k}) = \alpha + \beta e^{ik_x a} + \beta e^{-ik_x a} + \beta e^{ik_y a} + \beta e^{-ik_y a} + \beta e^{ik_z a} + \beta e^{-ik_z a} =$$

$$= \alpha + 2\beta(\cos k_x a + \cos k_y a + \cos k_z a)$$

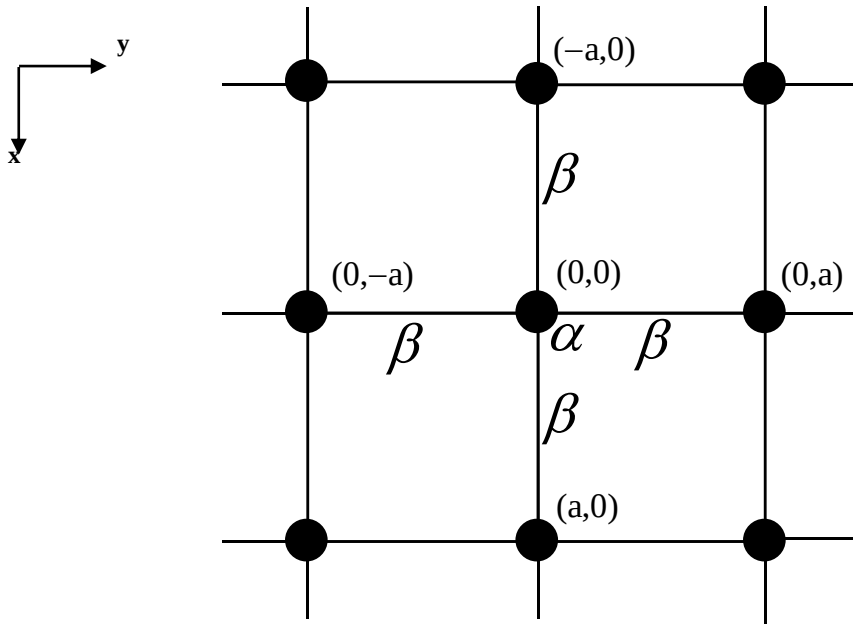


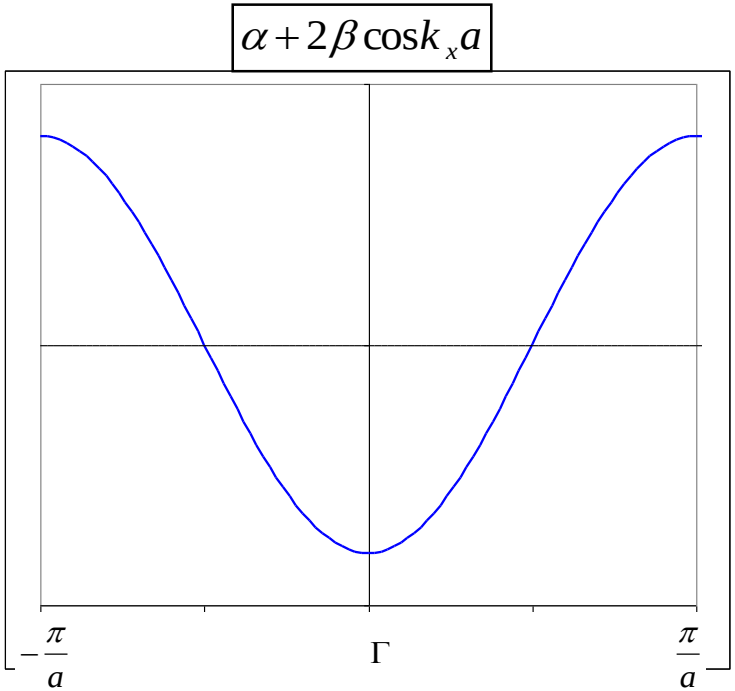

Formulas for the energy of band σ:

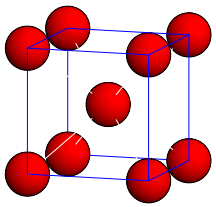

bcc: $E(\vec{k}) = \alpha + 8\beta \cos(k_x a)\cos(k_y a)\cos(k_z a)$

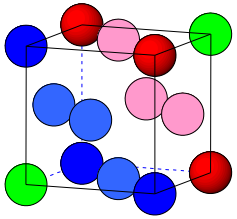

fcc (ccp): $E(\vec{k}) = \alpha + 4\beta[\cos(k_x a)\cos(k_y a) + \cos(k_y a)\cos(k_z a) + \cos(k_z a)\cos(k_x a)]$

hcp: $$E(\mathbf{k}) = \alpha + 2\beta\{\cos(k_x a) + 2\cos(\tfrac{1}{2}k_x a)\cos(\sqrt{\tfrac{3}{2}}k_y a) \pm \cos(k_z c)[1 + 4\cos^2(\tfrac{1}{2}k_x a) + 4\cos(\tfrac{1}{2}k_x a)\cos(\sqrt{\tfrac{3}{2}}k_y a)^{1/2}]\}$$

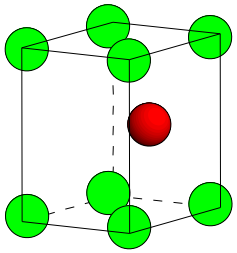

The calculation should includes energies of 3 exchange integrals: β(σ), β(π) and β(δ).
Their ratio is β(σ) : β(π) : β(δ) = 1 : 0.8 : 0.1

# Přechodné kovy

- Comparison of the energies of the structures fcc, hcp (only the ideal ratio a:c) and bcc
- The dependence of the energy on the cell volume is calculated for each structure and the minimum is selected.

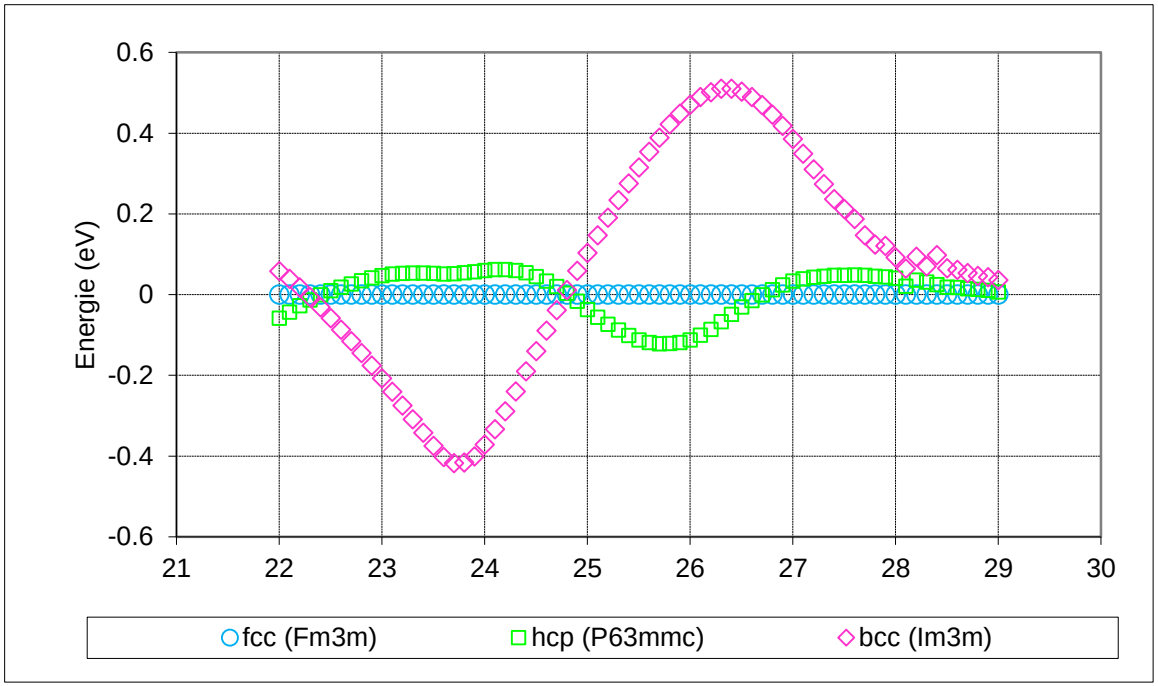


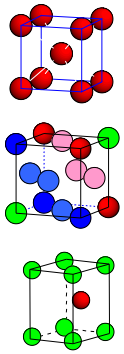

bcc

ccp (fcc)

hcp

| | 21 | 22 | 23 | 24 | 25 | 26 | 27 | 28 | 29 | 30 |
|---|---|---|---|---|---|---|---|---|---|---|
| 3d | Sc | Ti | V | Cr | Mn | Fe | Co | Ni | Cu | Zn |
| 4d | Y | Zr | Nb | Mo | Tc | Ru | Rh | Pd | Ag | Cd |
| 5d | Lu | Hf | Ta | W | Re | Os | Ir | Pt | Au | Hg |

Cr fcc (Fm3m) $3p^6 4s^2 3d^4$

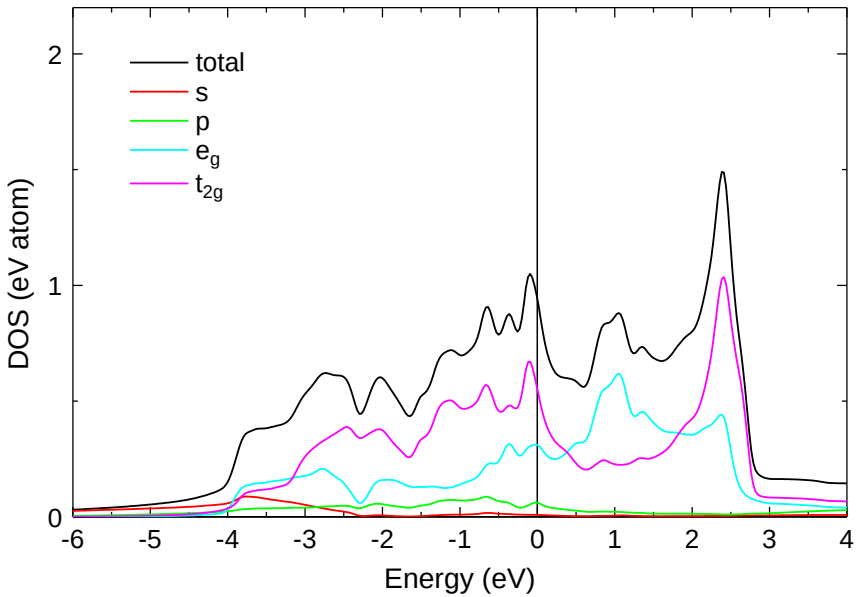


Ni fcc (Fm3m) $3p^6 4s^2 3d^8$

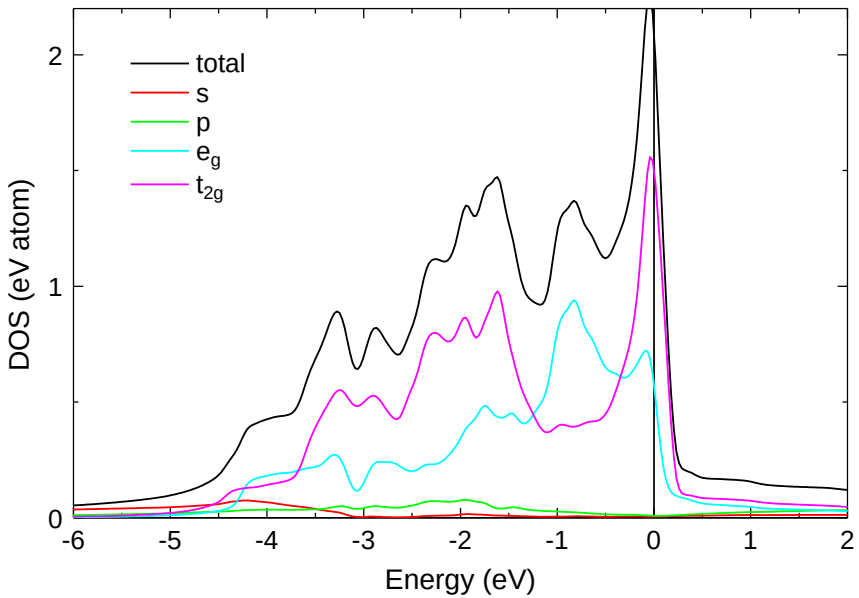

# Transition metals

Cr bcc (Im3m) $3p^6 4s^2 3d^4$

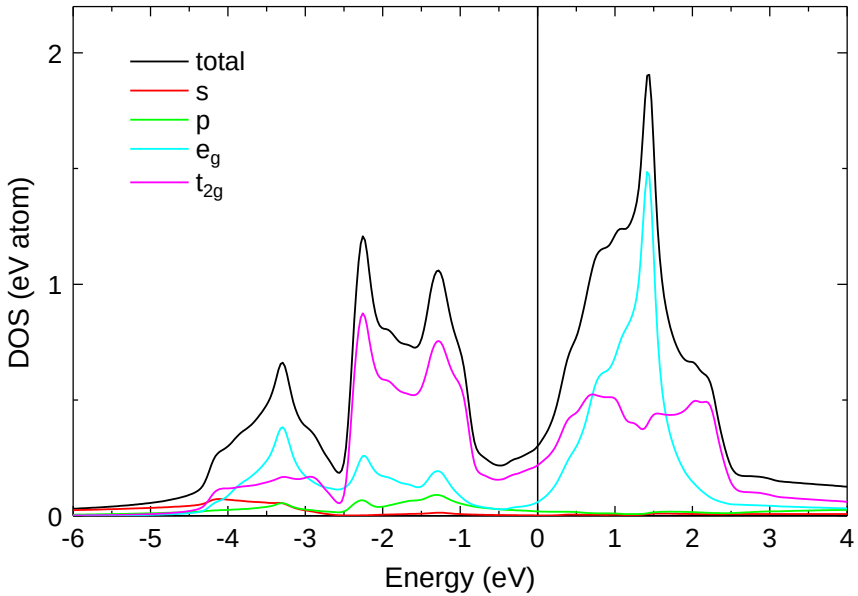


Ni bcc (Im3m) $3p^6 4s^2 3d^8$

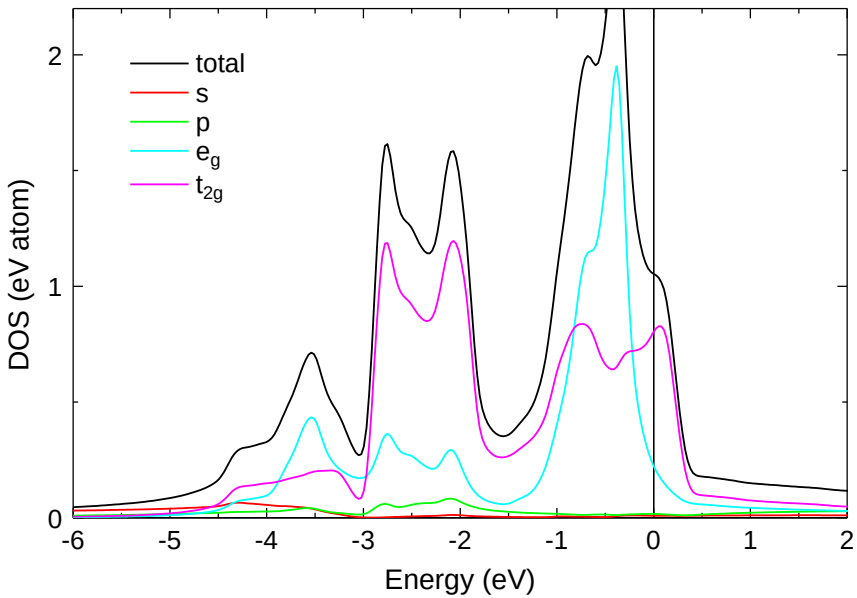

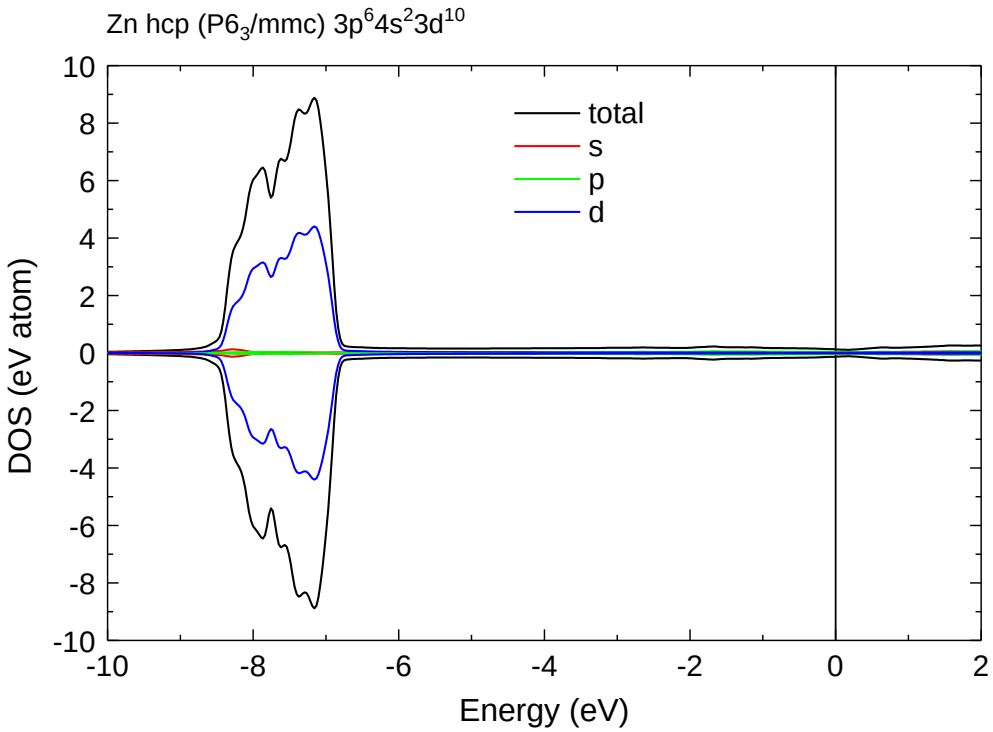
Zn hcp (P6$_3$/mmc) 3p$^6$4s$^2$3d$^{10}$
total
s
p
d
DOS (eV atom)
Energy (eV)
10
8
6
4
2
0
-2
-4
-6
-8
-10
-10
-8
-6
-4
-2
0
2

# sp-metals

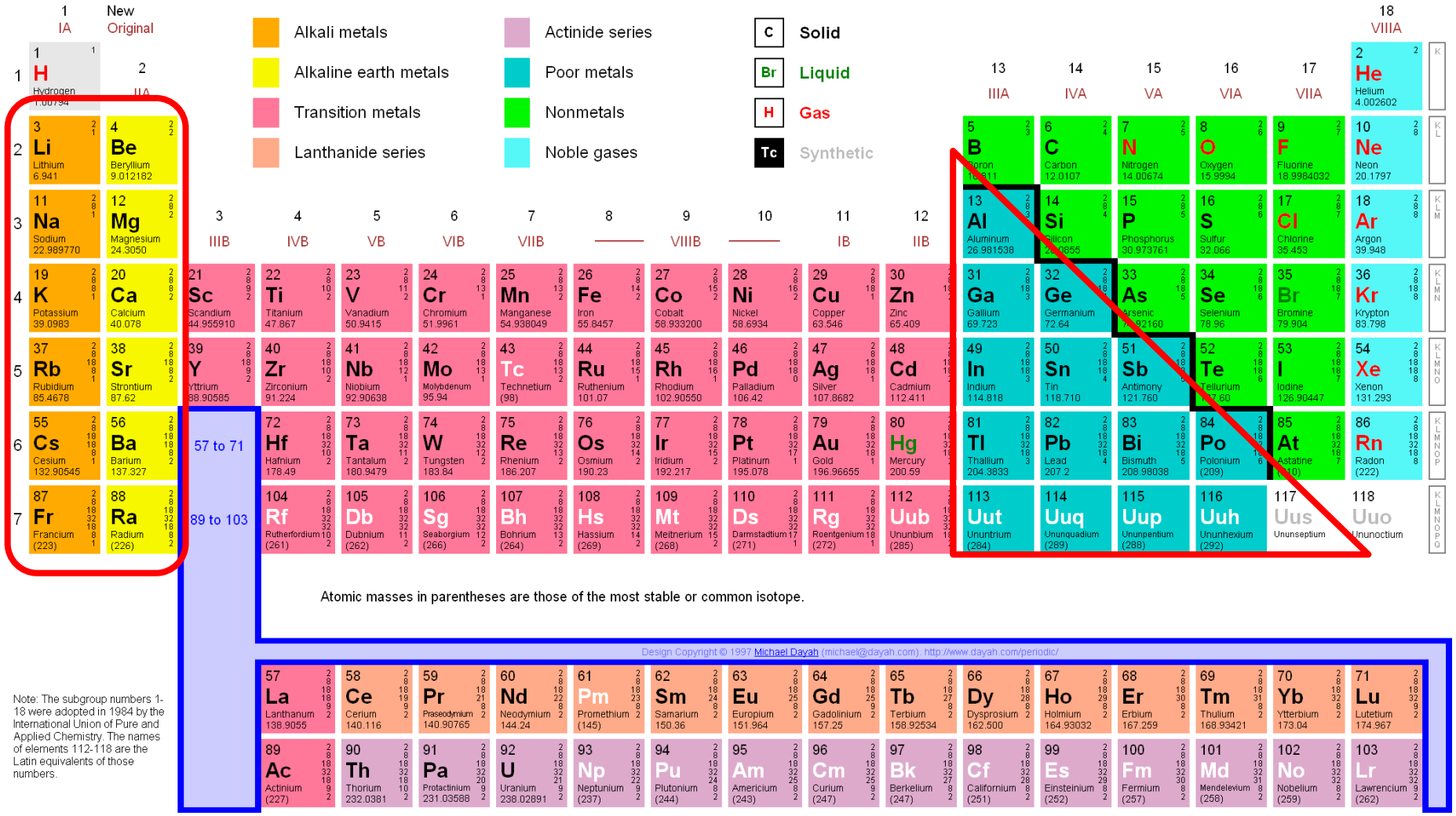


Note: The subgroup numbers 1-18 were adopted in 1984 by the International Union of Pure and Applied Chemistry. The names of elements 112-118 are the Latin equivalents of those numbers.

# sp-metals

| | I | II |
|---|---|---|
| 2 | Li | Be |
| 3 | Na | Mg |
| 4 | K | Ca |
| 5 | Rb | Sr |
| 6 | Cs | Ba |

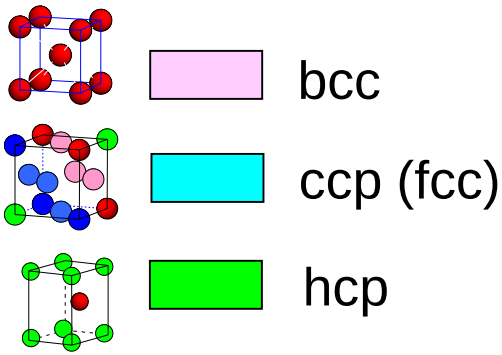


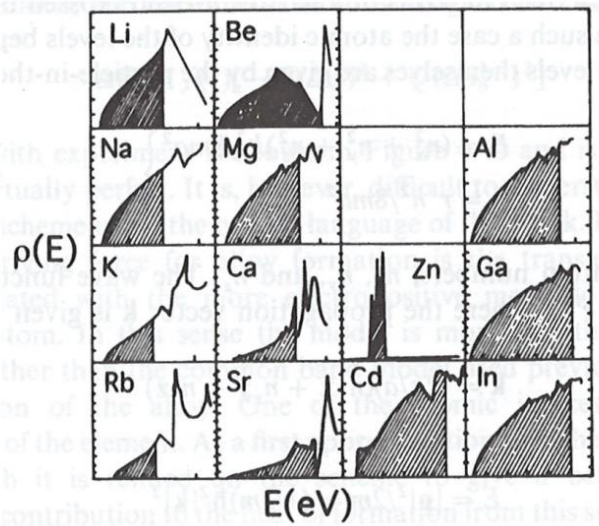


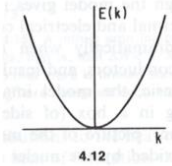


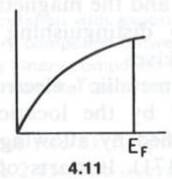


**Figure 4.41** Densities of states for some of the *sp* (main group) metals, showing the similarity for many to that expected from the free-electron model. (Adapted from Ref. 288.)

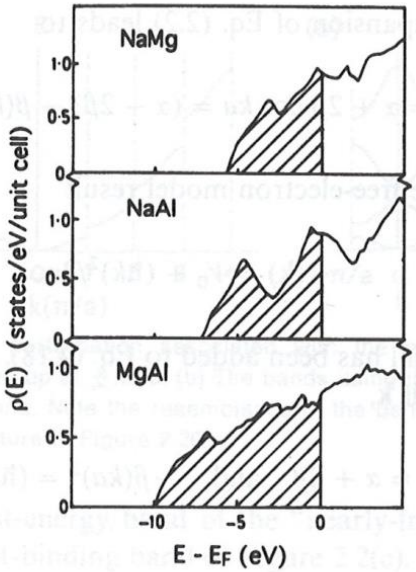


**Figure 4.42** Densities of states for some alloys of the *sp* (main group) metals. The poorest agreement with the free-electron parabola is seen for NaAl, where there is the largest difference in *Z* and hence electronegativity. (Adapted from Ref. 288.)

# diamond – Tight binding Hamiltonian

**Table 4.1** Hamiltonian matrix elements for the diamond structure

| | $s(C)$ | $s(A)$ | $p_x(C)$ | $p_y(C)$ | $p_z(C)$ | $p_x(A)$ | $p_y(A)$ | $p_z(A)$ |
|---|---|---|---|---|---|---|---|---|
| $s(C)$ | $e_s(C)$ | $V_{ss}g_0$ | 0 | 0 | 0 | $V_{sp}g_1$ | $V_{sp}g_2$ | $V_{sp}g_3$ |
| $s(A)$ | $V_{ss}g_0^*$ | $e_s(A)$ | $-V_{sp}g_1^*$ | $-V_{sp}g_2^*$ | $-V_{sp}g_3^*$ | 0 | 0 | 0 |
| $p_x(C)$ | 0 | $-V_{sp}g_1$ | $e_p(C)$ | 0 | 0 | $V_{xx}g_0$ | $V_{xy}g_3$ | $V_{xy}g_1$ |
| $p_y(C)$ | 0 | $-V_{sp}g_2$ | 0 | $e_p(C)$ | 0 | $V_{xy}g_3$ | $V_{xx}g_0$ | $V_{xy}g_1$ |
| $p_z(C)$ | 0 | $-V_{sp}g_3$ | 0 | 0 | $e_p(C)$ | $V_{xy}g_1$ | $V_{xy}g_2$ | $V_{xx}g_0$ |
| $p_x(A)$ | $V_{sp}g_1^*$ | 0 | $V_{xx}g_0^*$ | $V_{xy}g_3^*$ | $V_{xy}g_1^*$ | $e_p(A)$ | 0 | 0 |
| $p_y(A)$ | $V_{sp}g_2^*$ | 0 | $V_{xy}g_3^*$ | $V_{xx}g_0^*$ | $V_{xy}g_2^*$ | 0 | $e_p(A)$ | 0 |
| $p_z(A)$ | $V_{sp}g_3^*$ | 0 | $V_{xy}g_1^*$ | $V_{xy}g_1^*$ | $V_{xx}g_0^*$ | 0 | 0 | $e_p(A)$ |

$$\left.\begin{aligned}
\mathbf{d}_1 &= [111]a/4 \\
\mathbf{d}_2 &= [1\bar{1}\bar{1}]a/4 \\
\mathbf{d}_3 &= [\bar{1}1\bar{1}]a/4 \\
\mathbf{d}_4 &= [\bar{1}\bar{1}1]a/4
\end{aligned}\right\}$$

$$\left.\begin{aligned}
g_0(\mathbf{k}) &= e^{i\mathbf{k}\cdot\mathbf{d}_1} + e^{i\mathbf{k}\cdot\mathbf{d}_2} + e^{i\mathbf{k}\cdot\mathbf{d}_3} + e^{i\mathbf{k}\cdot\mathbf{d}_4} \\
g_1(\mathbf{k}) &= e^{i\mathbf{k}\cdot\mathbf{d}_1} + e^{i\mathbf{k}\cdot\mathbf{d}_2} - e^{i\mathbf{k}\cdot\mathbf{d}_3} - e^{i\mathbf{k}\cdot\mathbf{d}_4} \\
g_2(\mathbf{k}) &= e^{i\mathbf{k}\cdot\mathbf{d}_1} - e^{i\mathbf{k}\cdot\mathbf{d}_2} + e^{i\mathbf{k}\cdot\mathbf{d}_3} - e^{i\mathbf{k}\cdot\mathbf{d}_4} \\
g_3(\mathbf{k}) &= e^{i\mathbf{k}\cdot\mathbf{d}_1} - e^{i\mathbf{k}\cdot\mathbf{d}_2} - e^{i\mathbf{k}\cdot\mathbf{d}_3} + e^{i\mathbf{k}\cdot\mathbf{d}_4}
\end{aligned}\right\}$$

# diamond, wurtzite, sphalerite

sphalerite ZnS, diamond, Si

wurtzite ZnS

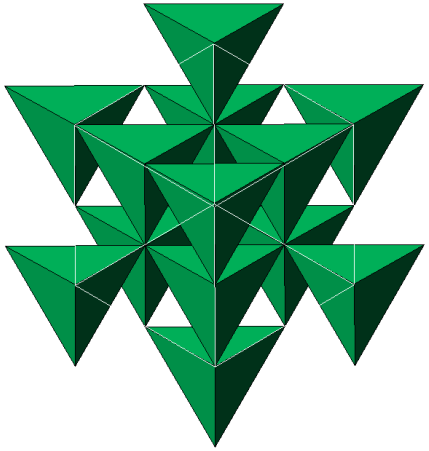

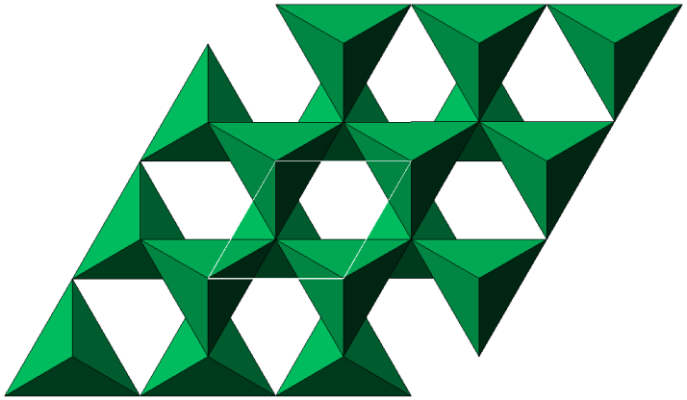

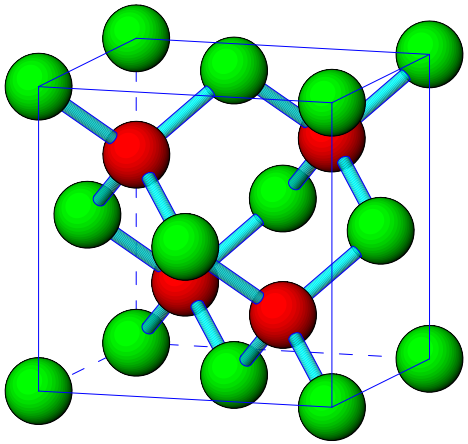

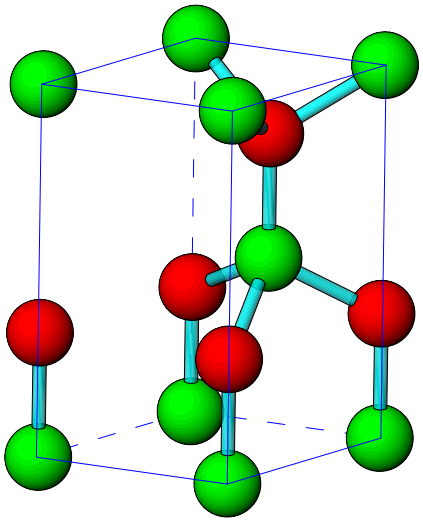

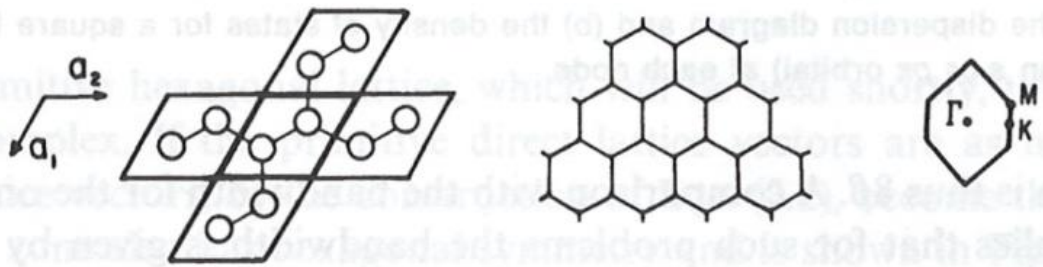


3.5

in 3.5 the secular determinant becomes

$$\begin{vmatrix} \alpha - E & \beta\{\exp[i\mathbf{k}\cdot(\frac{2}{3}\mathbf{a}_1 + \frac{1}{3}\mathbf{a}_2)] + \exp[i\mathbf{k}\cdot(\frac{1}{3}\mathbf{a}_1 - \frac{2}{3}\mathbf{a}_2)] + \exp[i\mathbf{k}\cdot(\frac{1}{3}\mathbf{a}_1 + \frac{1}{3}\mathbf{a}_2)] \\ H_{12}^* & \alpha - E \end{vmatrix} = 0 \tag{3.7}$$

with roots $E = \alpha \pm A^{1/2}\beta$, where

$$A = [3 + 2\cos(\mathbf{a}_1 + \mathbf{a}_2)\cdot\mathbf{k} + 2\cos\mathbf{a}_3\cdot\mathbf{k} + 2\cos\mathbf{a}_1\cdot\mathbf{k})] \tag{3.8}$$

# Molecular orbitals of the octahedra TM-O in perovskite

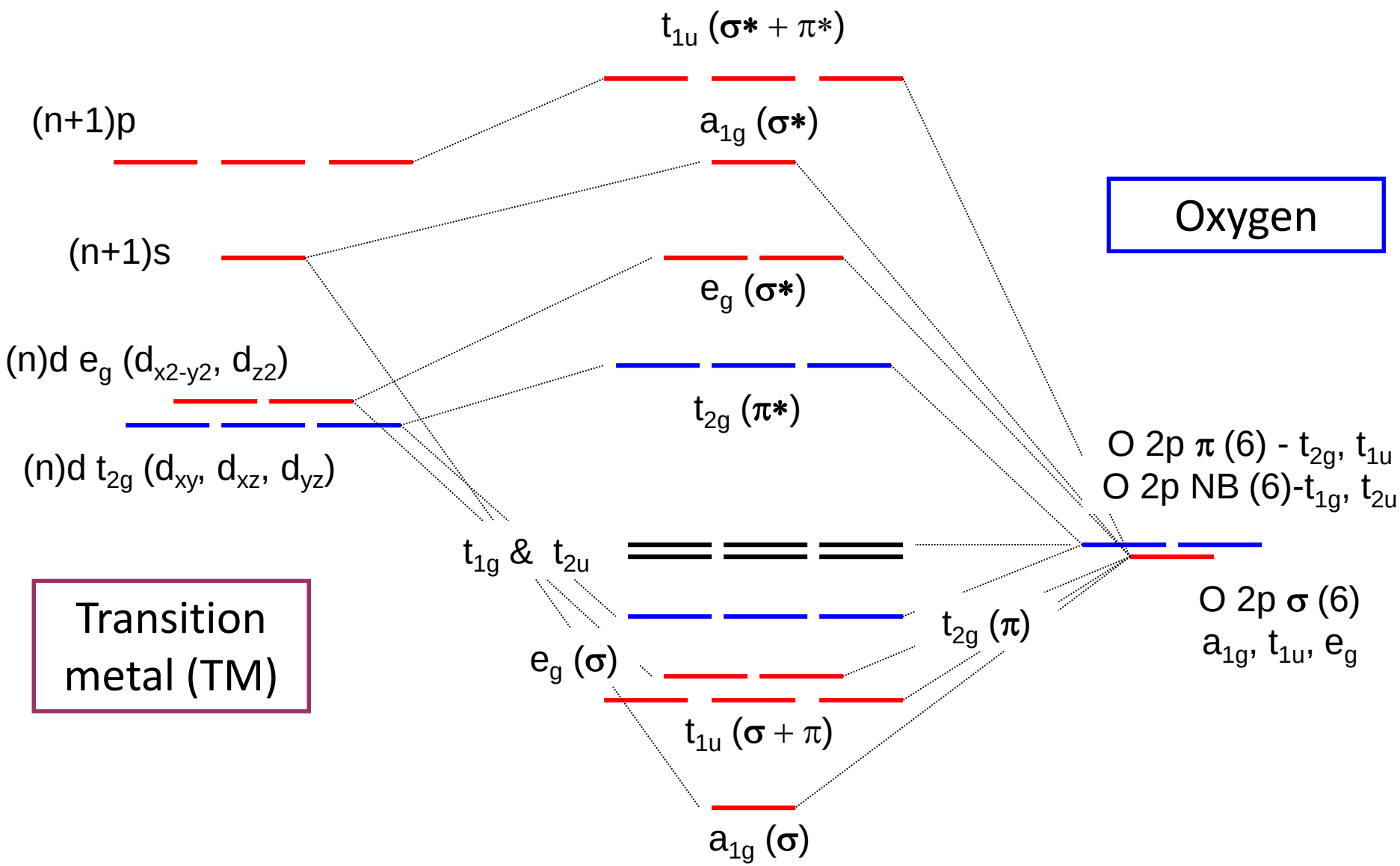

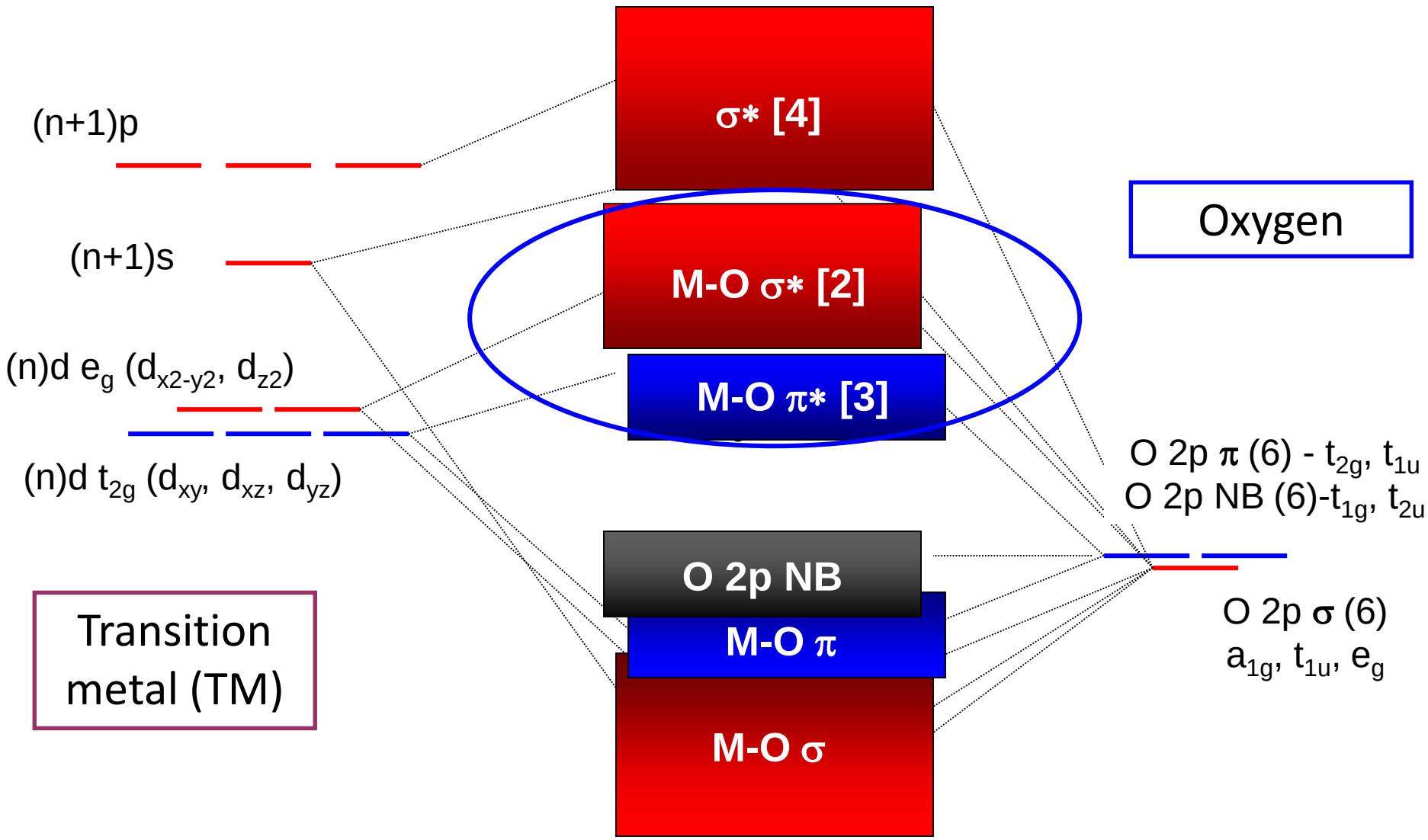
(n+1)p
(n+1)s
(n)d $e_g$ ($d_{x2-y2}$, $d_{z2}$)
(n)d $t_{2g}$ ($d_{xy}$, $d_{xz}$, $d_{yz}$)
Transition metal (TM)
σ* [4]
M-O σ* [2]
M-O π* [3]
O 2p NB
M-O π
M-O σ
Oxygen
O 2p π (6) - $t_{2g}$, $t_{1u}$
O 2p NB (6)-$t_{1g}$, $t_{2u}$
O 2p σ (6)
$a_{1g}$, $t_{1u}$, $e_g$

X point ($k_x=\pi/a$, $k_y=k_z=0$)

$d_{xy}$, $d_{xz}$ → anti-bonding

$d_{yz}$ → non-bonding

2 degenerate bands

M point ($k_x=k_y=\pi/a$, $k_z=0$)

$d_{xy}$, → anti-bonding

$d_{yz}$, $d_{xz}$ → less anti-bonding

2 degenerate bands

R point ($k_x=k_y=k_z=\pi/a$)

$d_{xy}$, $d_{yz}$, $d_{xz}$ → anti-bonding

3 degenerate bands

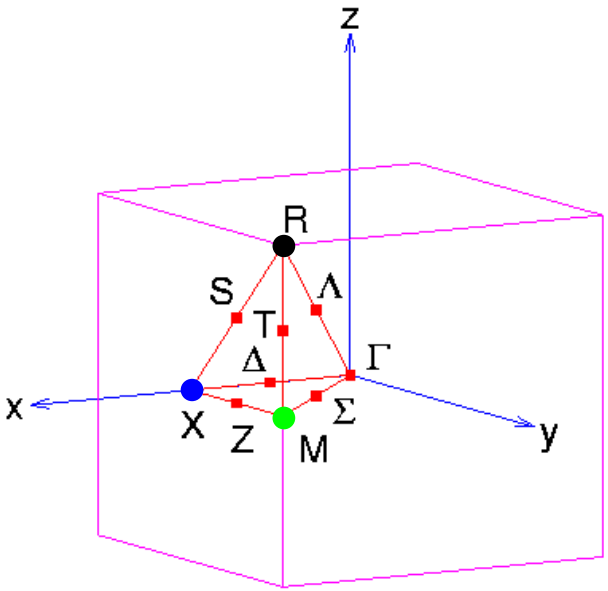


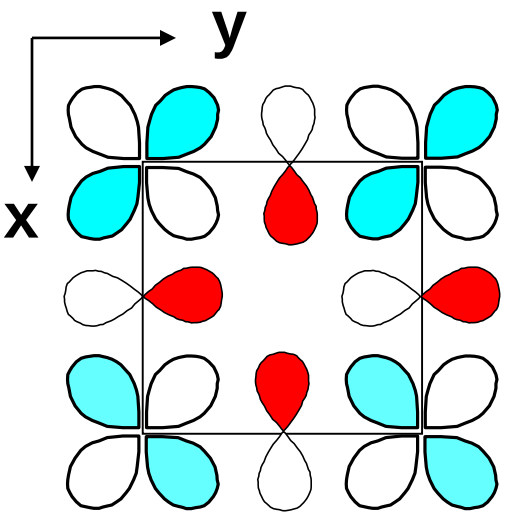


X point

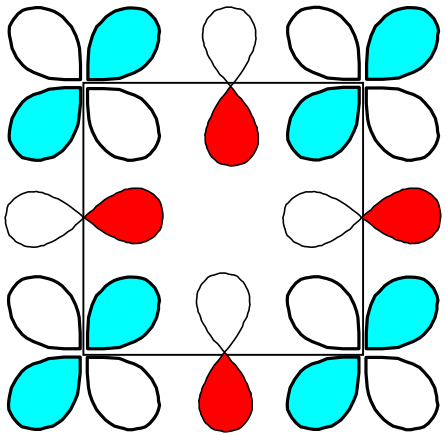

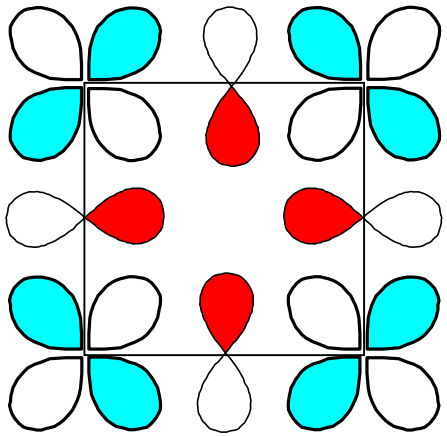

$\Gamma$ point
($k_x$=$k_y$=0)
Non-bonding

$\mathbf{M}$ point
($k_x$=$k_y$=$\pi$/a)
Anit-bonding

$\pi^*$ - overlap (TM $t_{2g}$ – O 2p $\pi$)
$\Gamma \rightarrow \mathrm{M}$ :
Band energy is increasing

Bigger overlap for $\sigma$ bond
$W(\sigma^*) > W(\pi^*)$

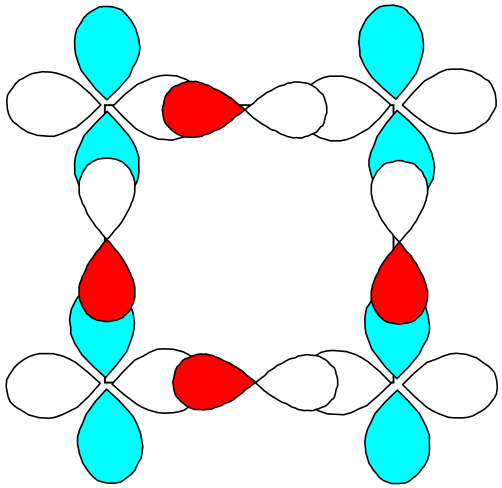

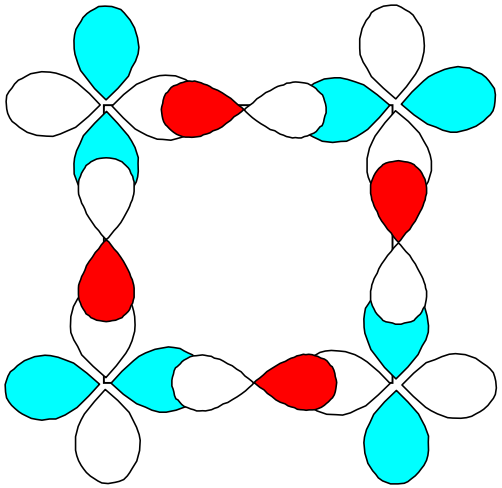

$\sigma^*$ - overlap (TM $e_g$ – O 2p $\sigma$)
$\Gamma \rightarrow \mathrm{M}$ :
Band energy is increasing

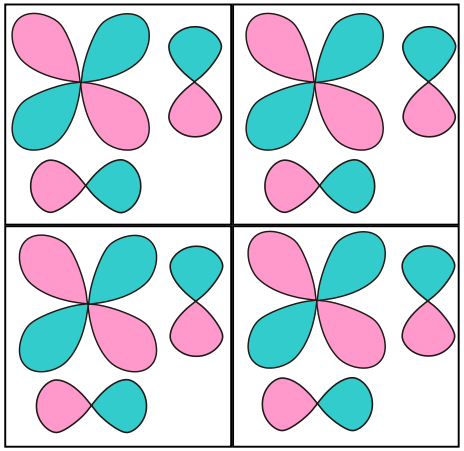

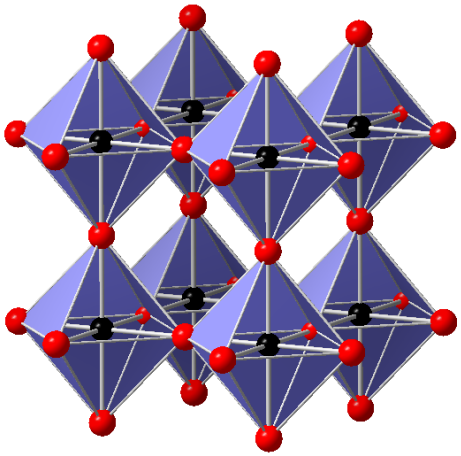

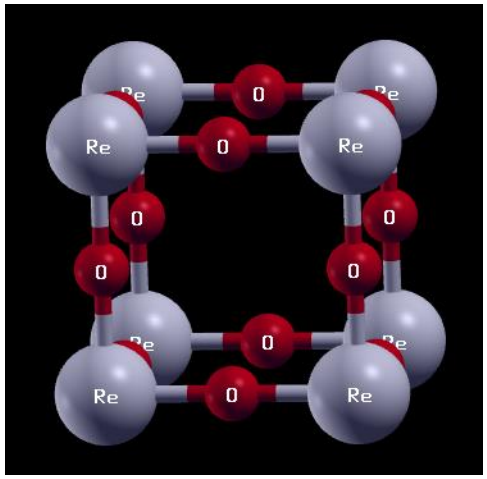


$ReO_3$:

$Re^{6+}$ $d^1$

$\pi$-bonds $t_{2g}$ - p

$d_{xy}$ – $p_x(y)$, $p_y(x)$

$d_{xz}$ – $p_x(z)$, $p_z(x)$

$d_{yz}$ – $p_y(z)$, $p_z(y)$

# Band structure of $ReO_3$ – comparison of DFT a TB

DFT

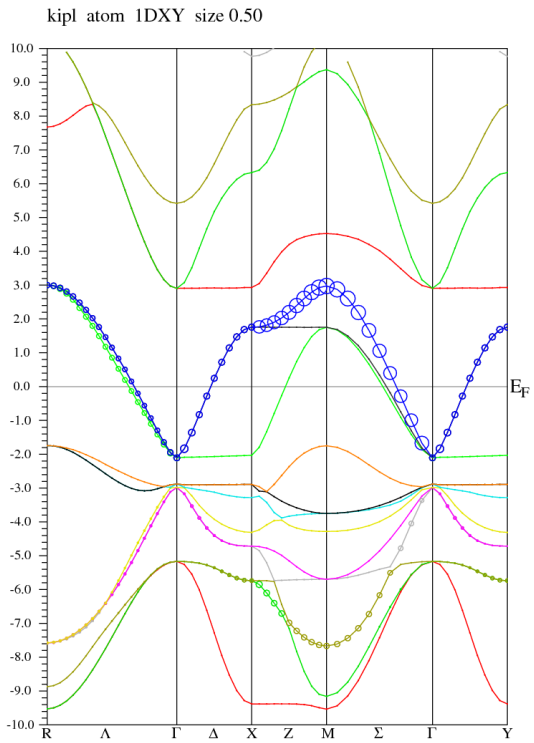
kipl atom 1DXY size 0.50

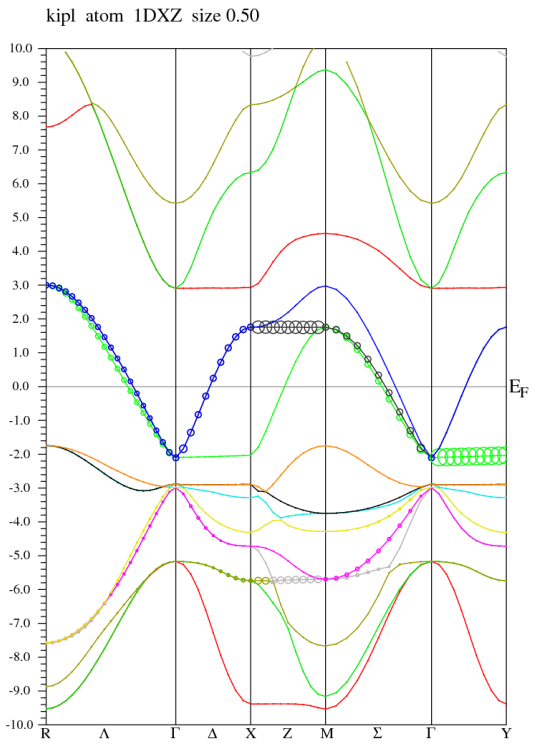
kipl atom 1DXZ size 0.50

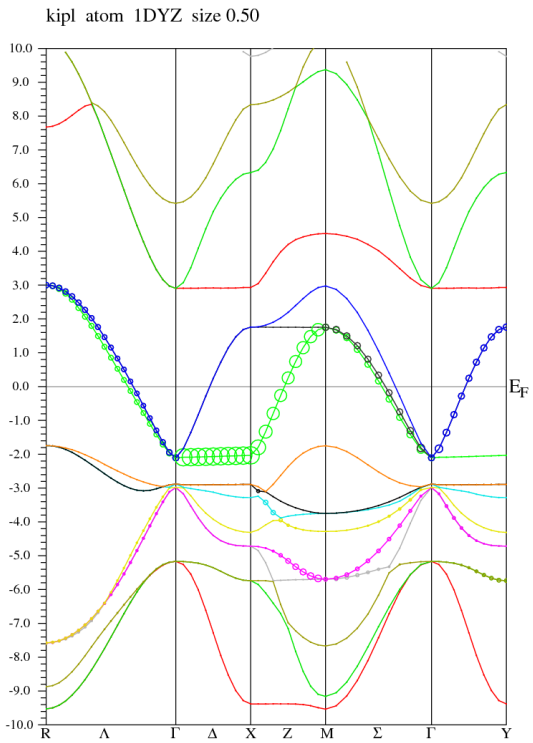
kipl atom 1DYZ size 0.50

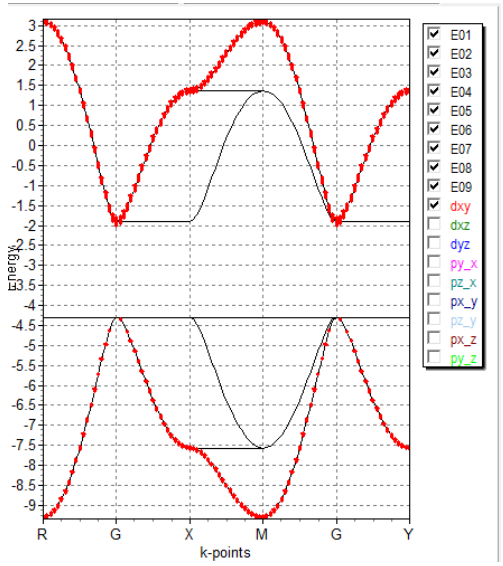

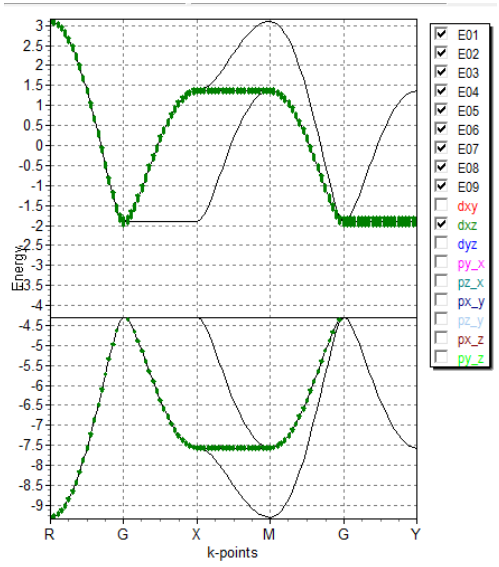

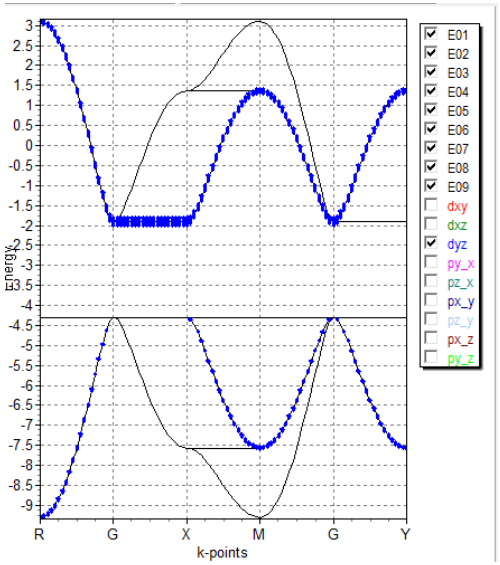

# $d_{xy} - p_x, p_y$

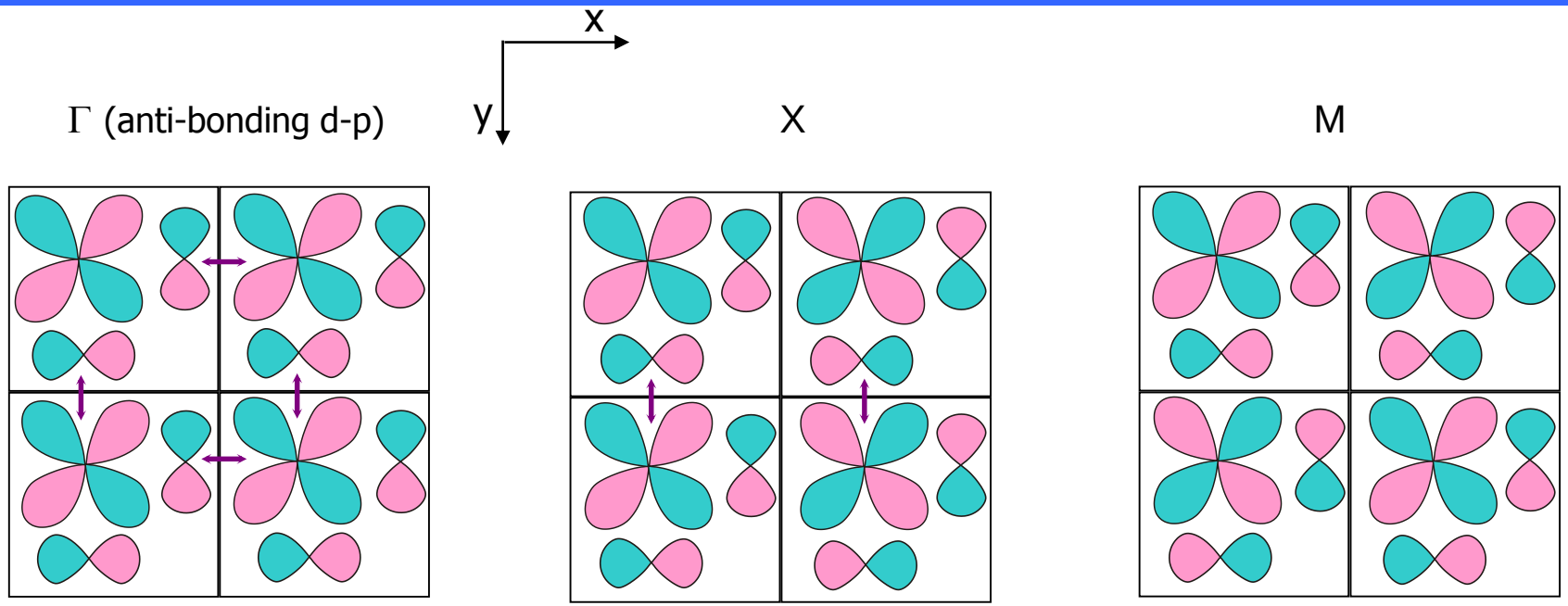


$$\begin{matrix} 1 & 1 \\ 1 & 1 \end{matrix} \qquad \begin{matrix} 1 & -1 \\ 1 & -1 \end{matrix} \qquad \begin{matrix} 1 & -1 \\ -1 & 1 \end{matrix}$$

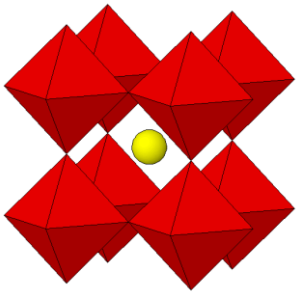

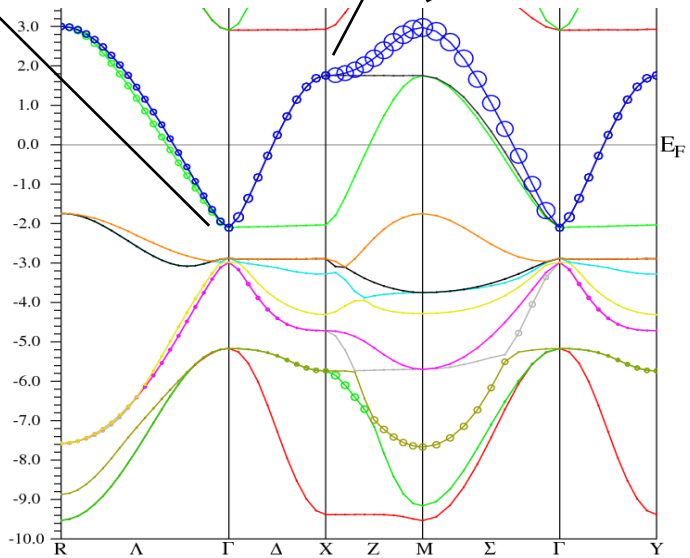


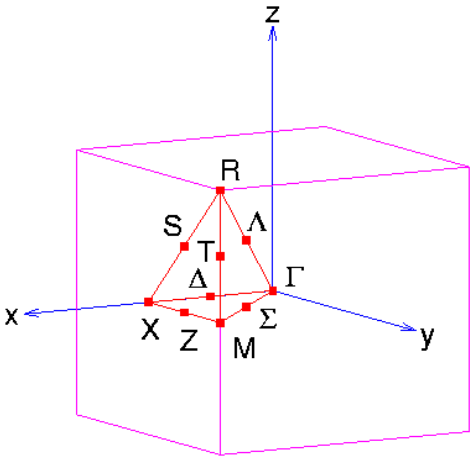

# Lowering of symmetry – octahedral tilting

Cubic perovskite (Pm3m)

Bond angle Mn-O-Mn = 180°

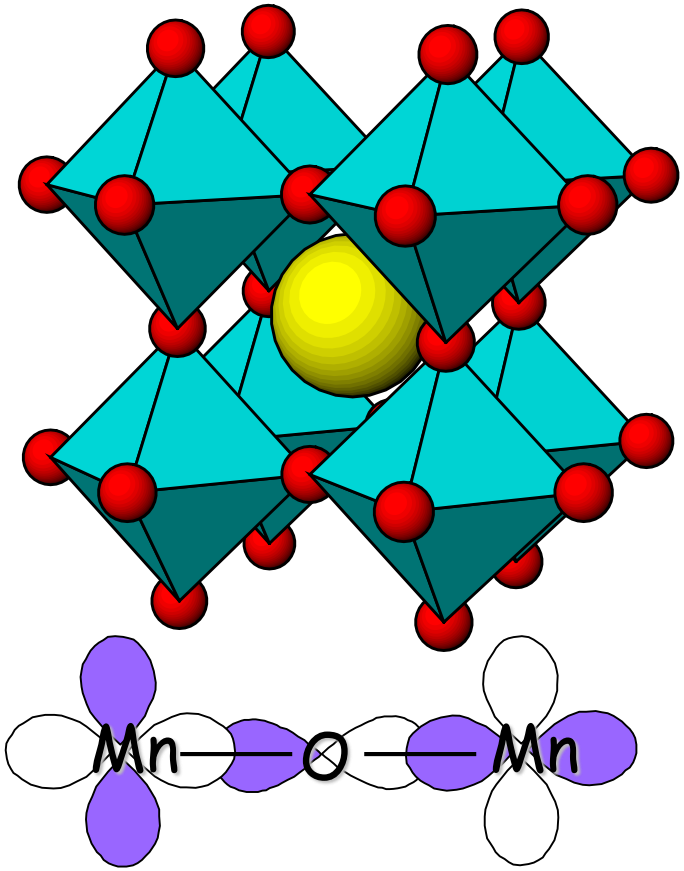


Orthorhombic perovskite (Pnma)

Bond angle Mn-O-Mn < 180°

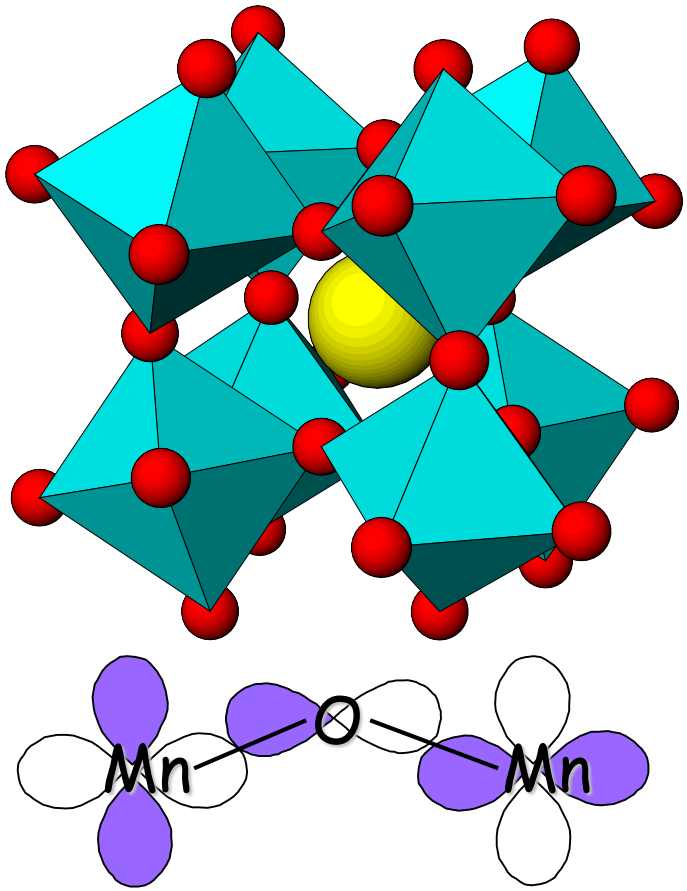

# Snížení symetrie – náklon oktaedrů

Cubic perovskite (Pm3m)
Bond angle Mn-O-Mn = 180°

Orthorhombic perovskite (Pnma)
Bond angle Mn-O-Mn < 180°

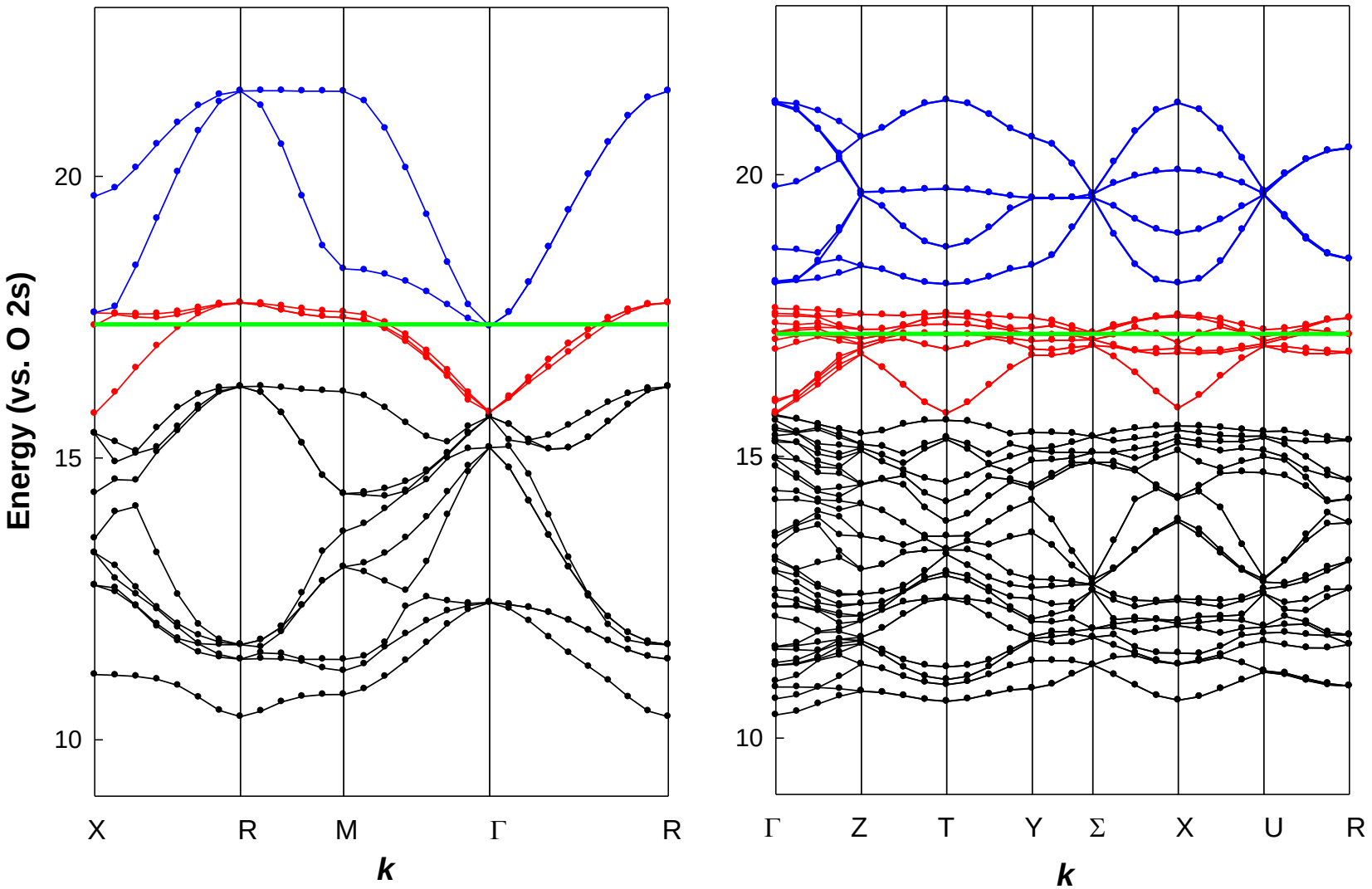

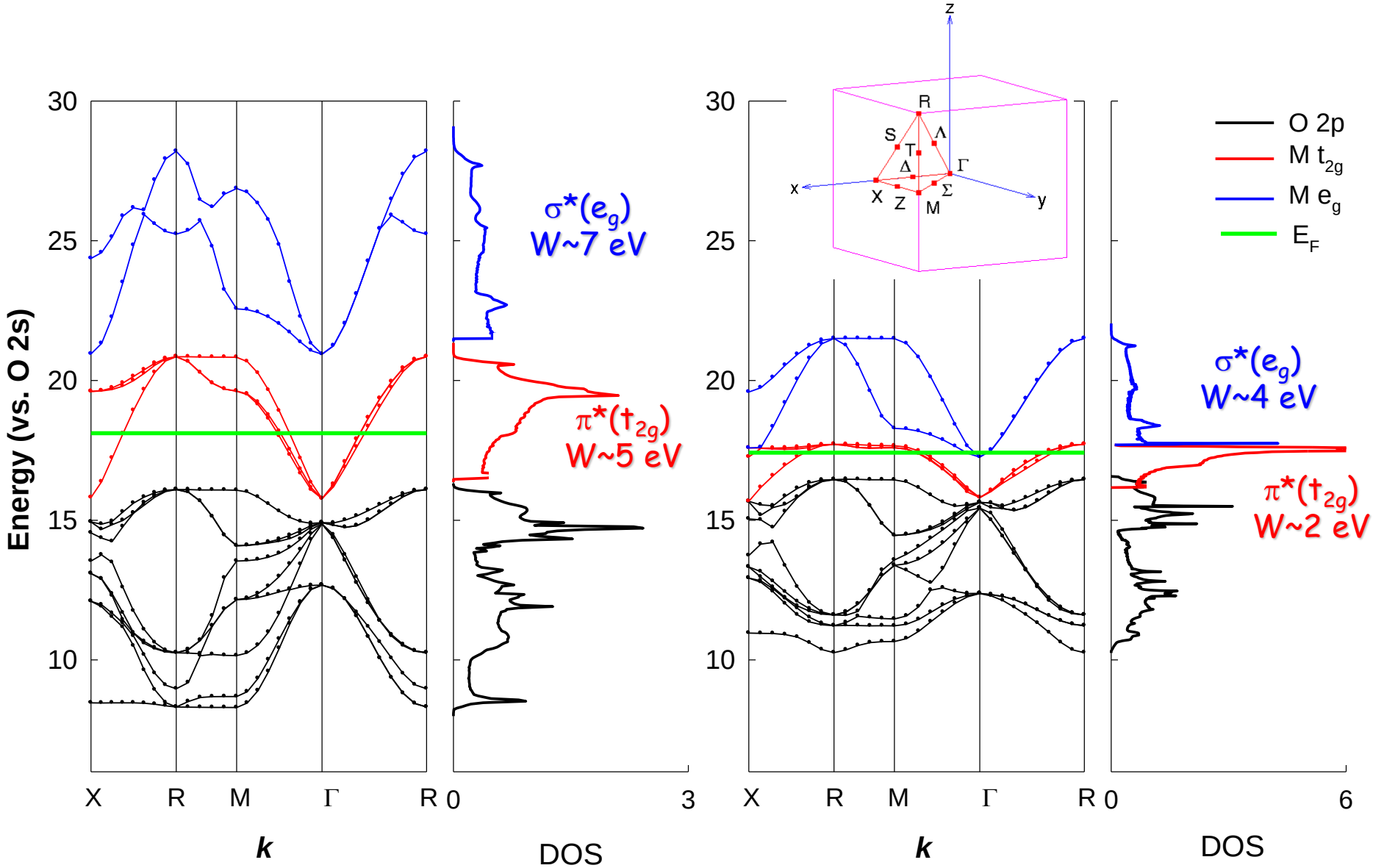
Energy (vs. O 2s)
30
25
20
15
10
X R M Γ R
k
0 3
DOS
σ*(eg)
W~7 eV
π*(t2g)
W~5 eV
z
x
y
R
S
Λ
T
Δ
Γ
X
Z
M
Σ
O 2p
M t2g
M eg
EF
σ*(eg)
W~4 eV
π*(t2g)
W~2 eV
0 6

$ReO_3$

$MnO_3^{2-}$

- Diagram of molecular orbitals for octahedra
- $\pi^*(t_{2g})$ and $\sigma^*(e_g)$ bands
- Overlap of orbitals and band width ($ReO_3$ vs. $MnO_3^{2-}$)
- Structural deformation (octahedral tilting)
- Exchange energy (Energy of spin pairing)
- Number of d-electrons

$LaCrO_3$

$d^3 – t_{2g}^3$

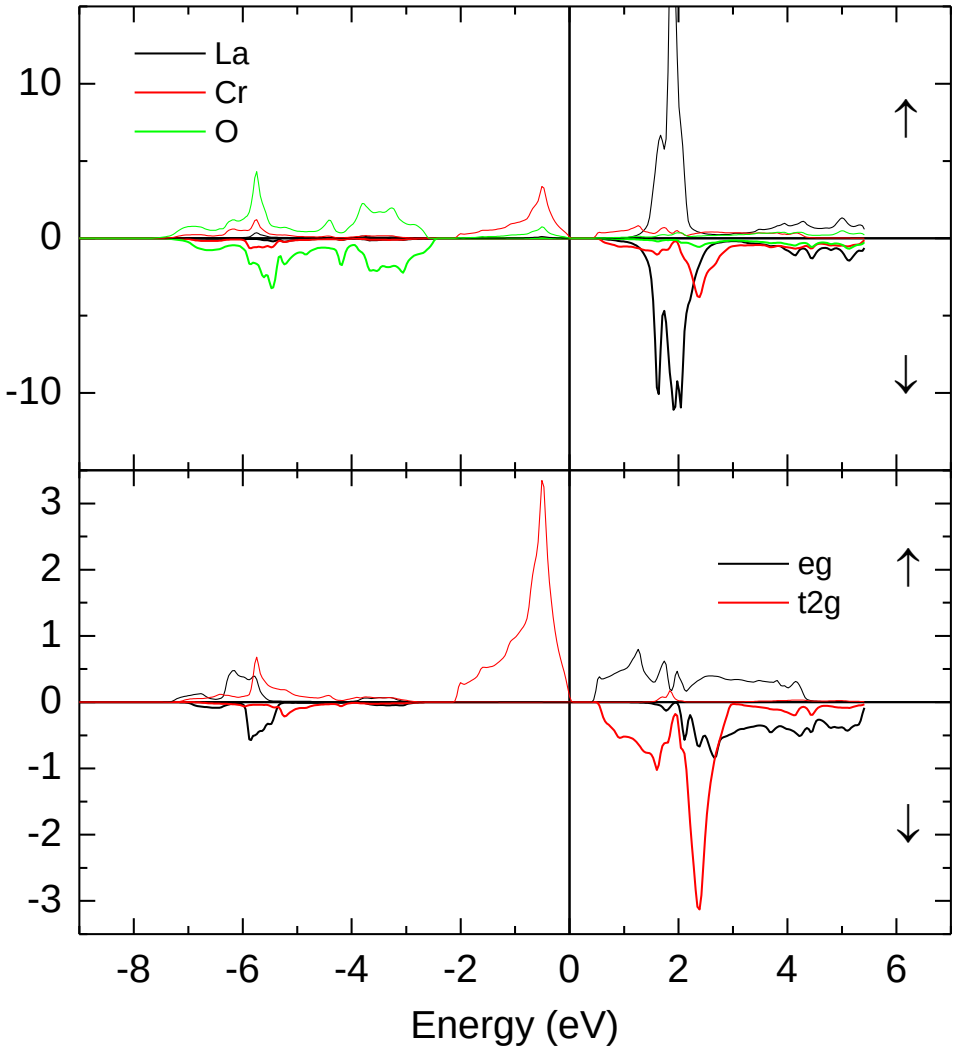


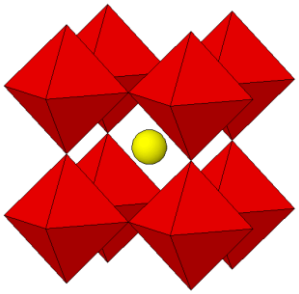

# $LaCrO_3$ – Cr-$d^3$ : $t_{2g}$ band

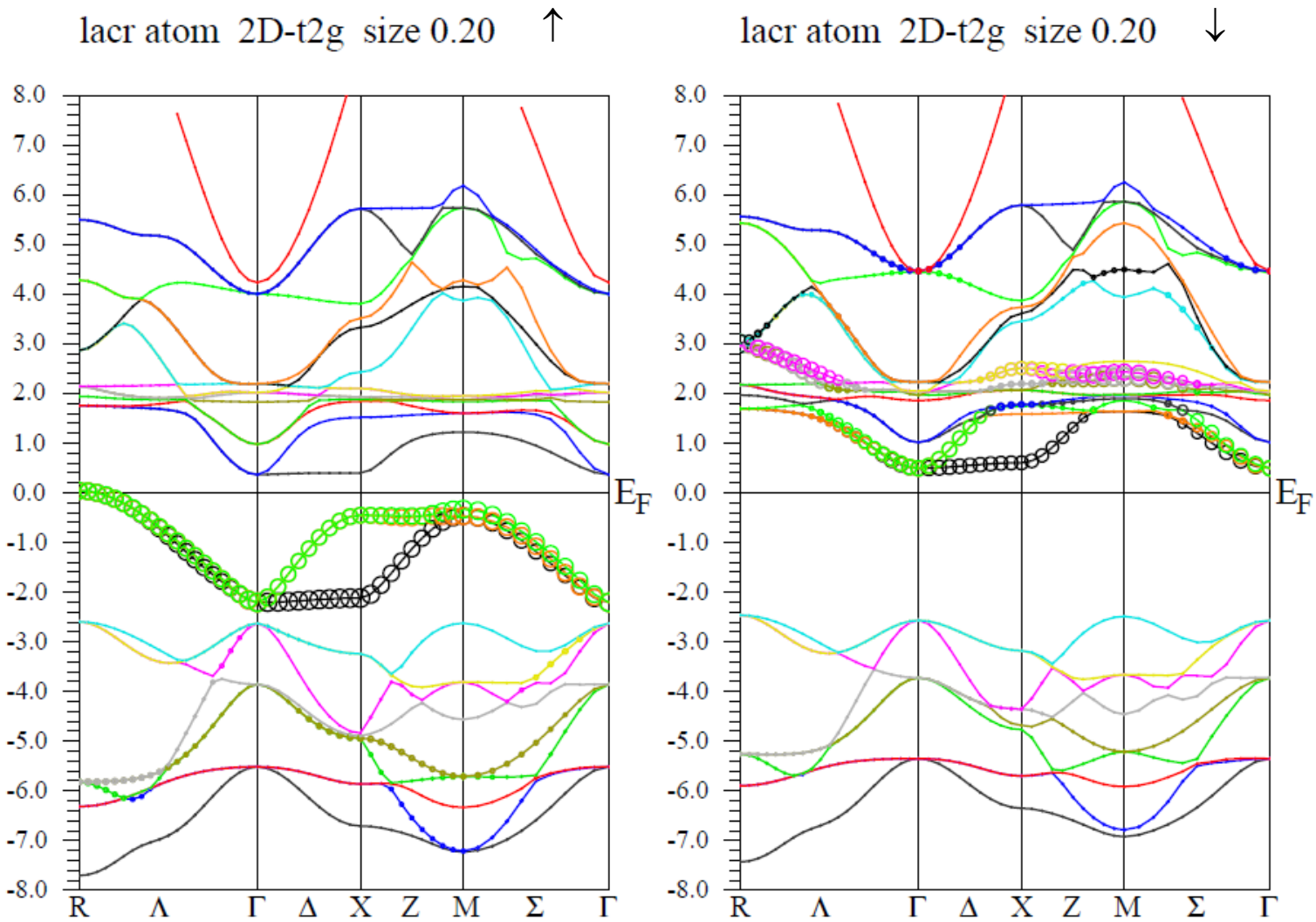


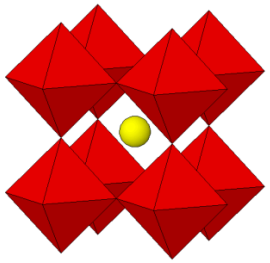

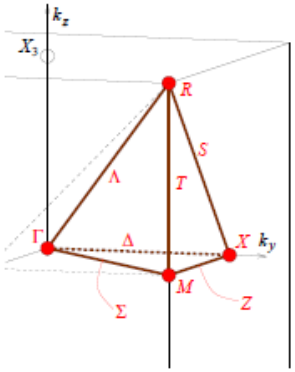


Figure 1: $LaCrO_3$, $d^3 - t_{2g}^3$, Cr-$t_{2g}$

# $LaCrO_3$ – Cr-$d^3$ : $t_{2g}$ bands ($d_{xy}$, $d_{xz}$, $d_{yz}$)

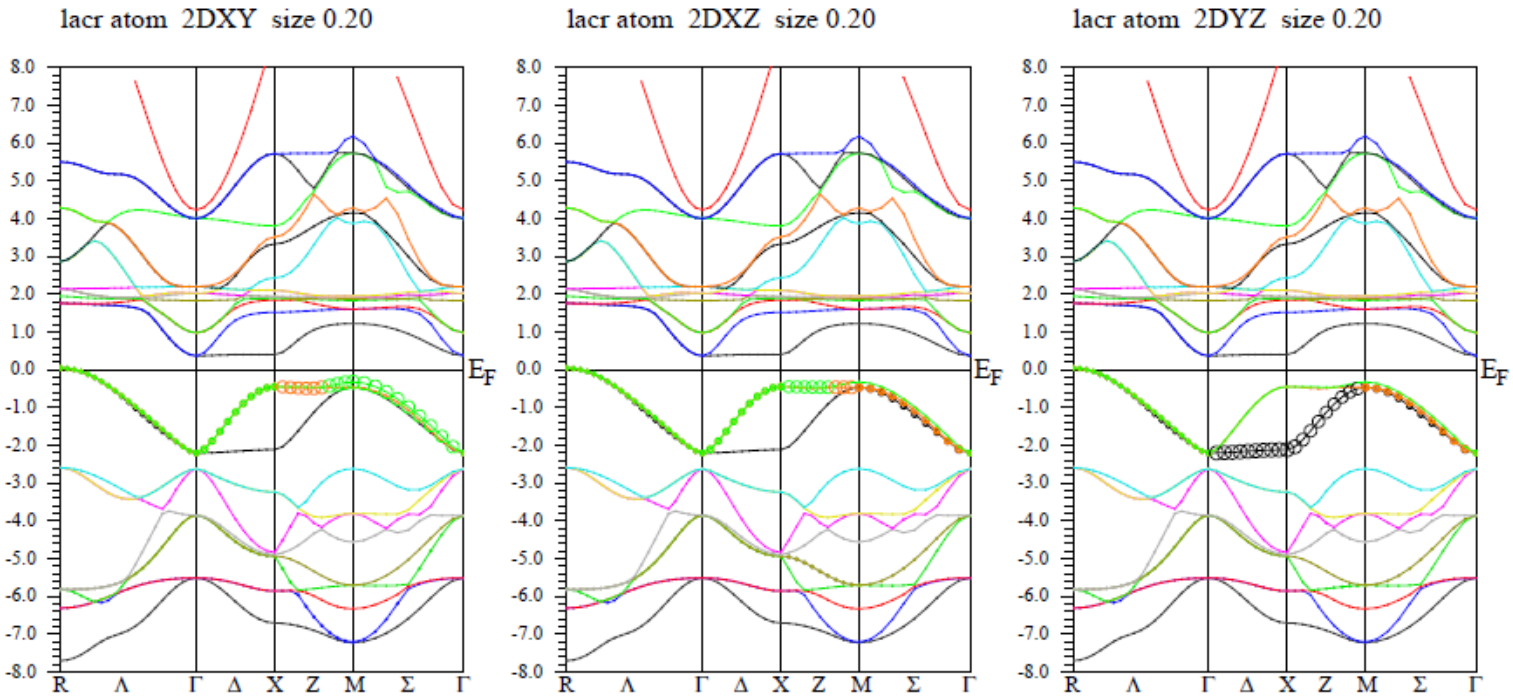


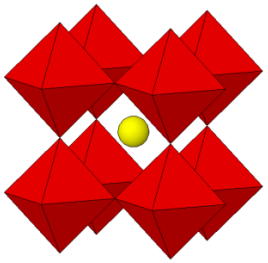

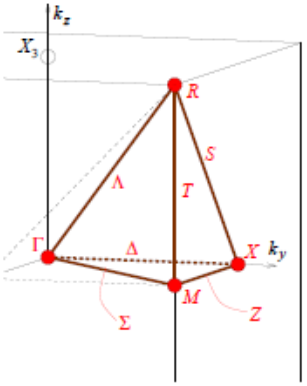


Figure 2: $LaCrO_3$, $d^3 - t_{2g}^3$, Cr-$t_{2g}$

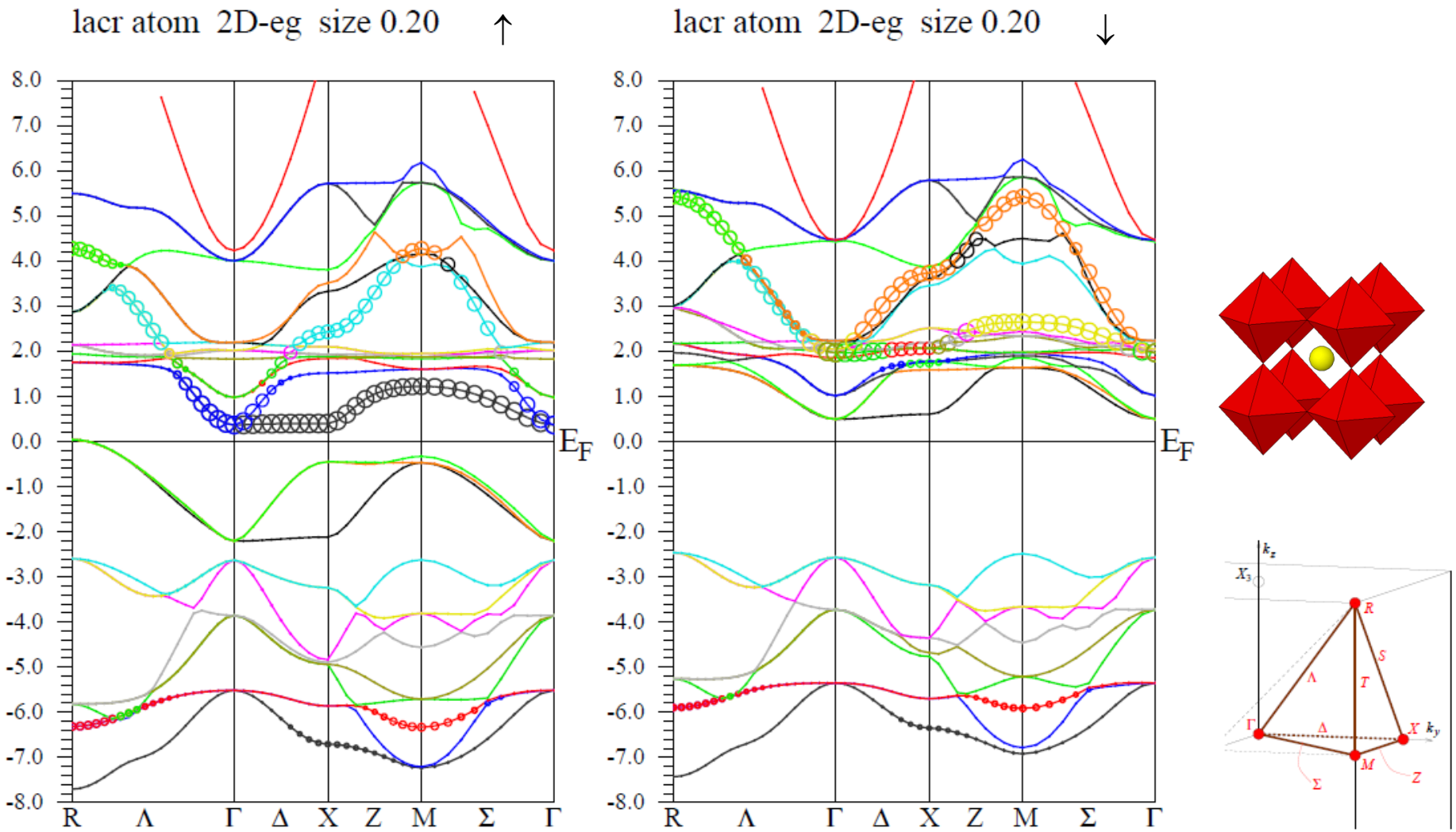


Figure 3: $LaCrO_3$, $d^3 - t_{2g}^3$, Cr-$e_g$

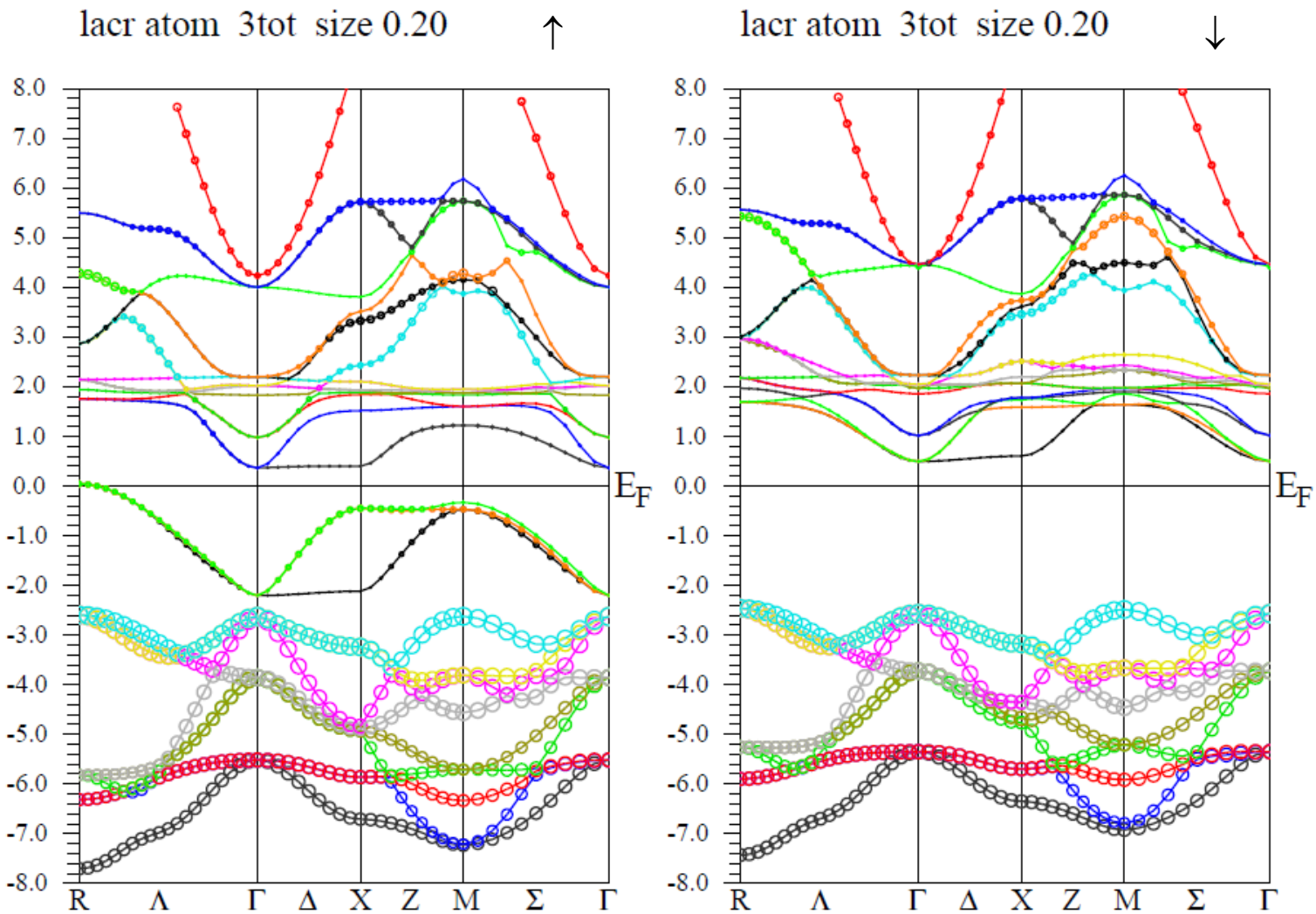


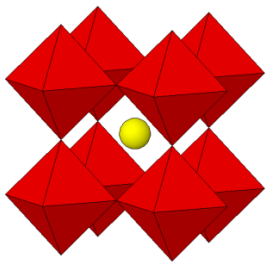

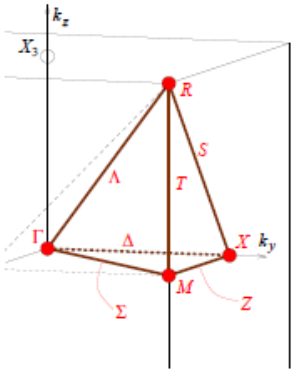


Figure 4: $LaCrO_3$, $d^3 - t_{2g}^3$, O

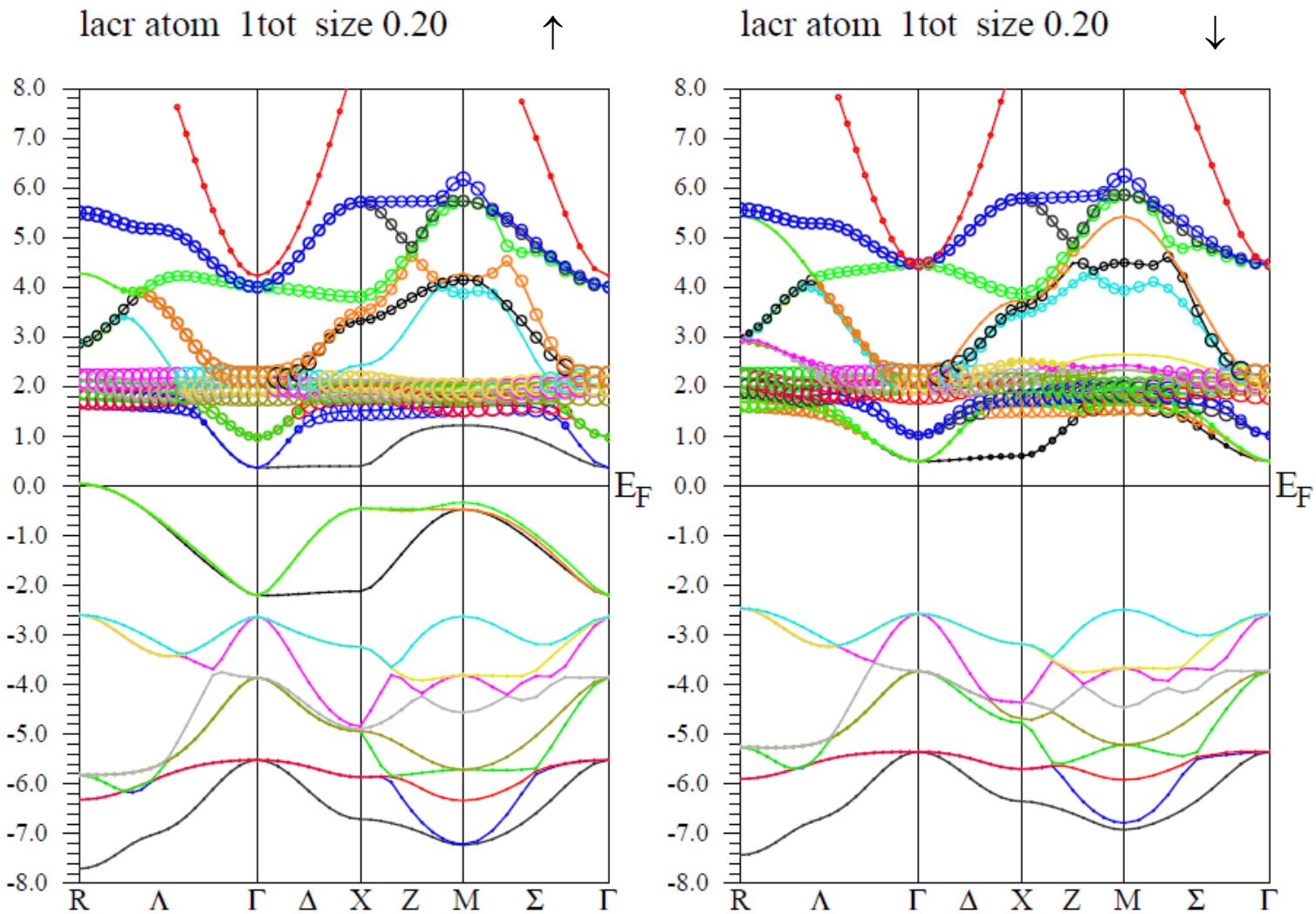


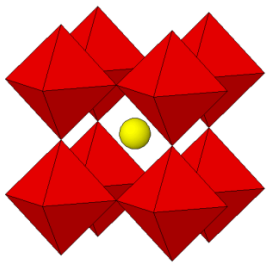

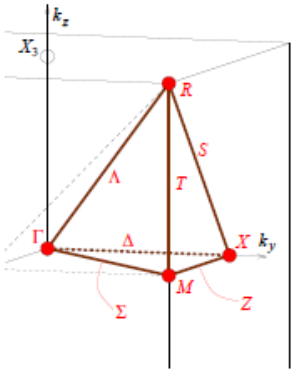


Figure 5: $LaCrO_3$, $d^3 - t_{2g}^3$, La

$LaFeO_3$
$d^5$ – $t_{2g}^3 e_g^2$
high spin

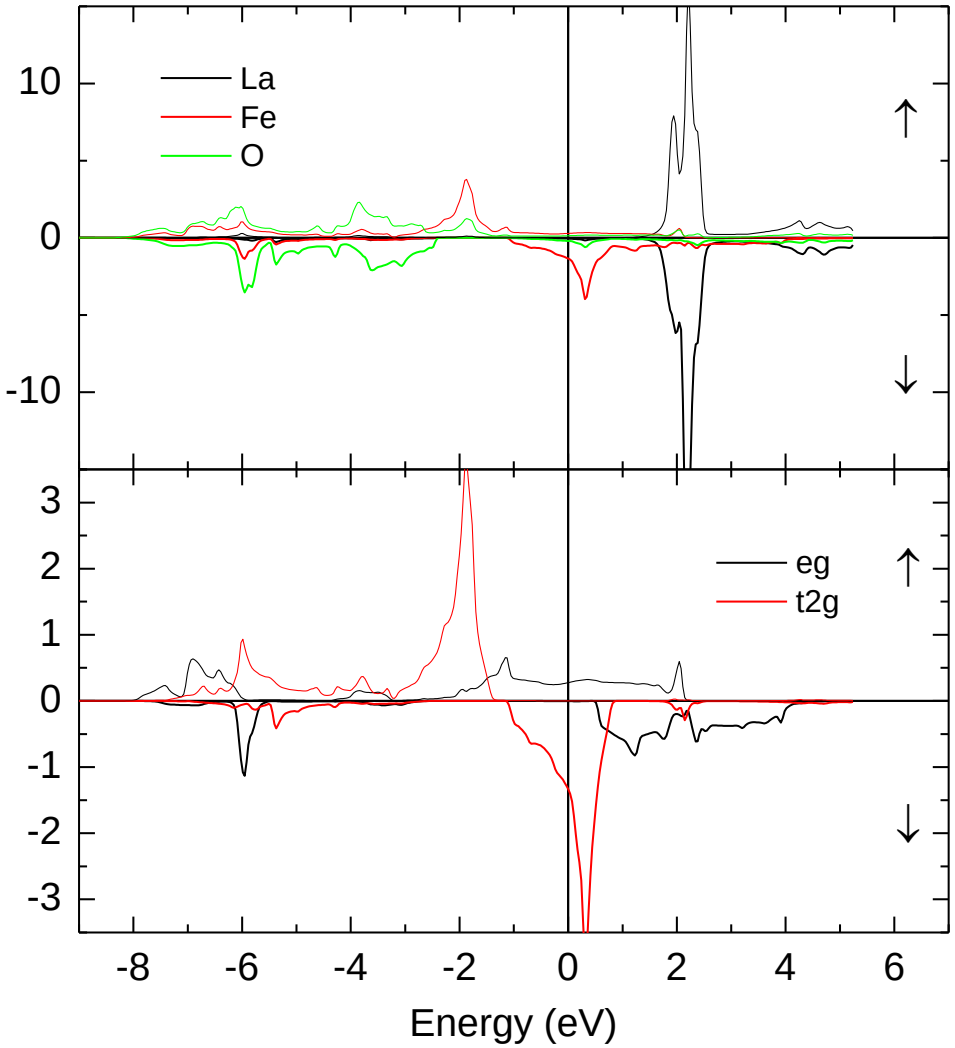


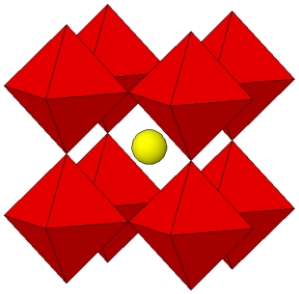

$LaNiO_3$

$d^7 – t_{2g}^6 e_g^1$

low spin

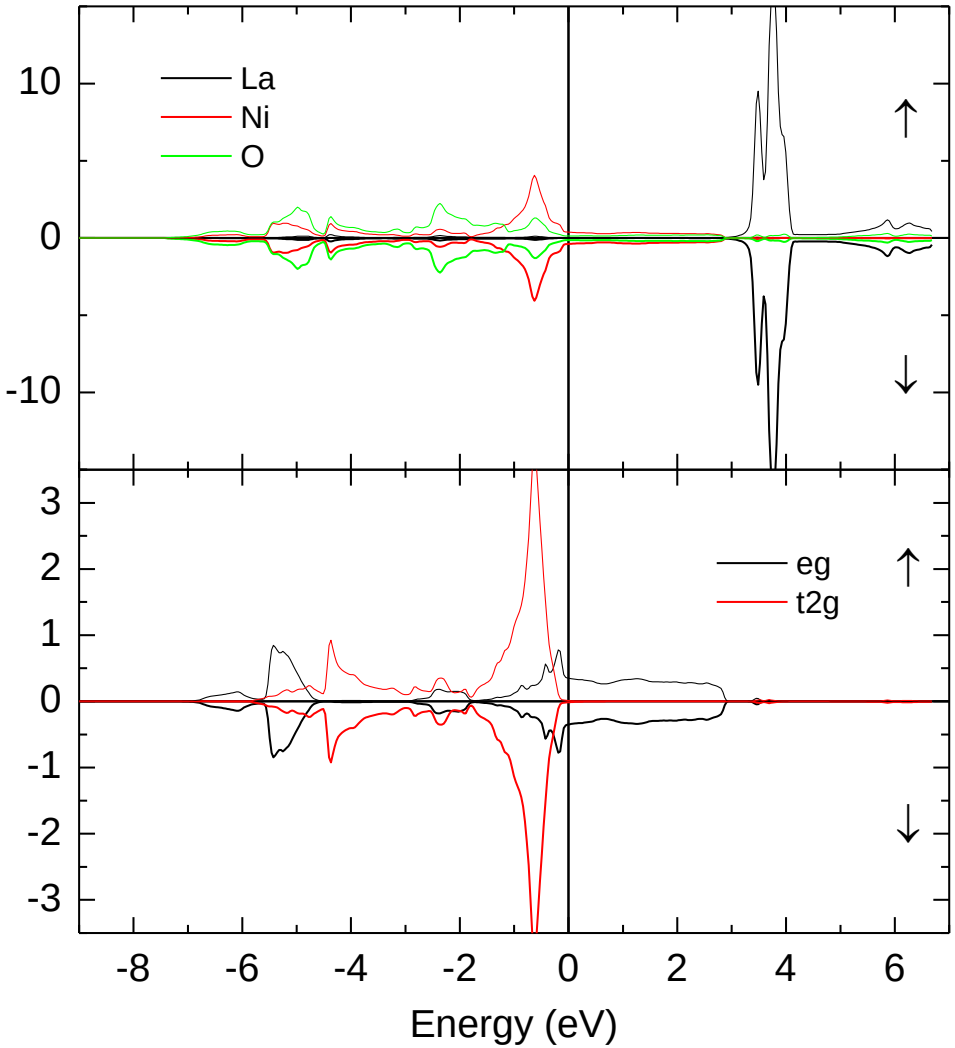


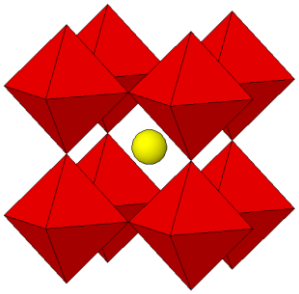

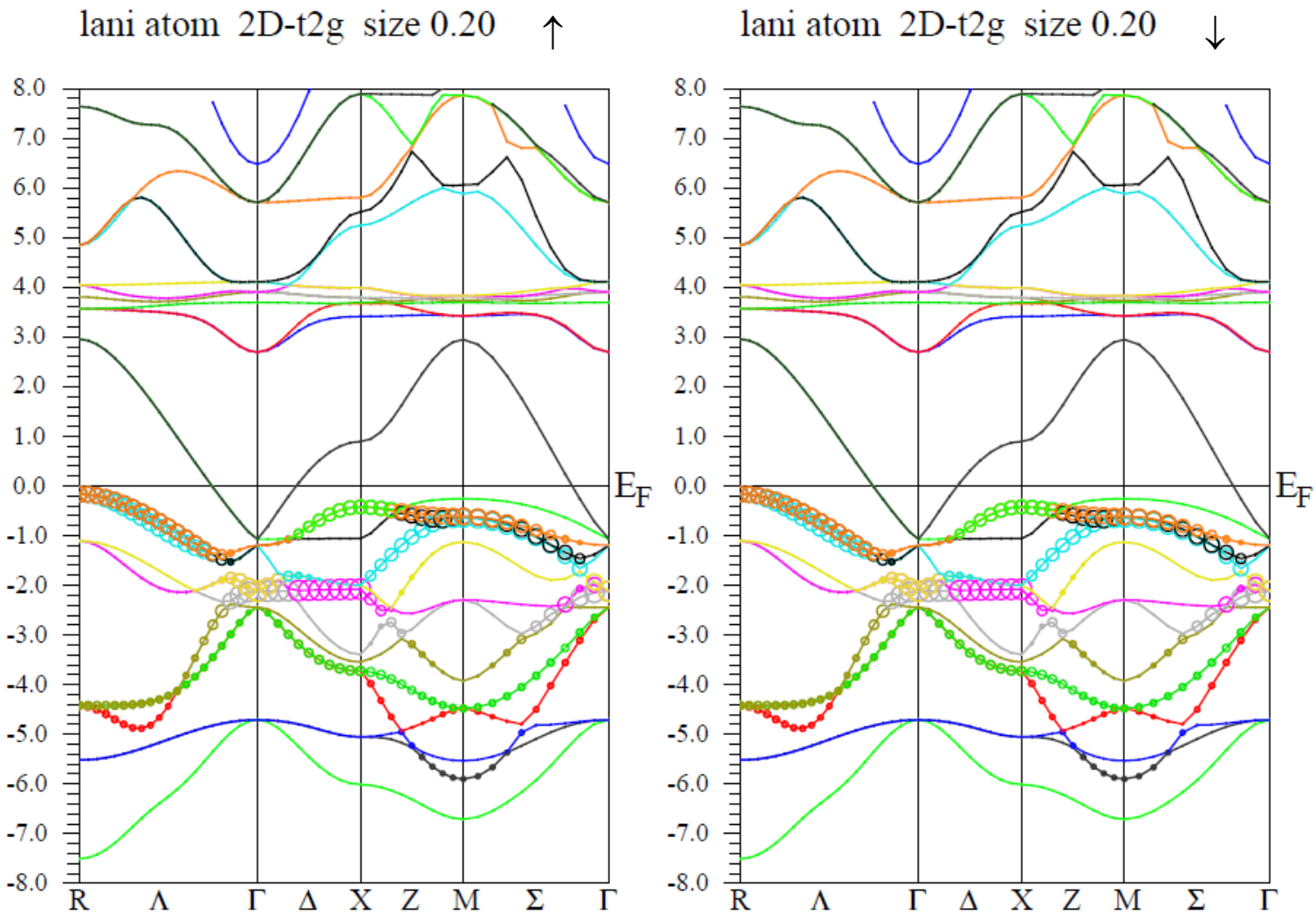


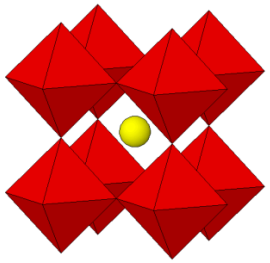

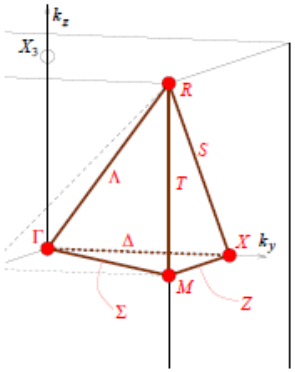


Figure 6: $LaNiO_3$, $d^7 - t_{2g}^6 e_g^1$, Ni-$t_{2g}$

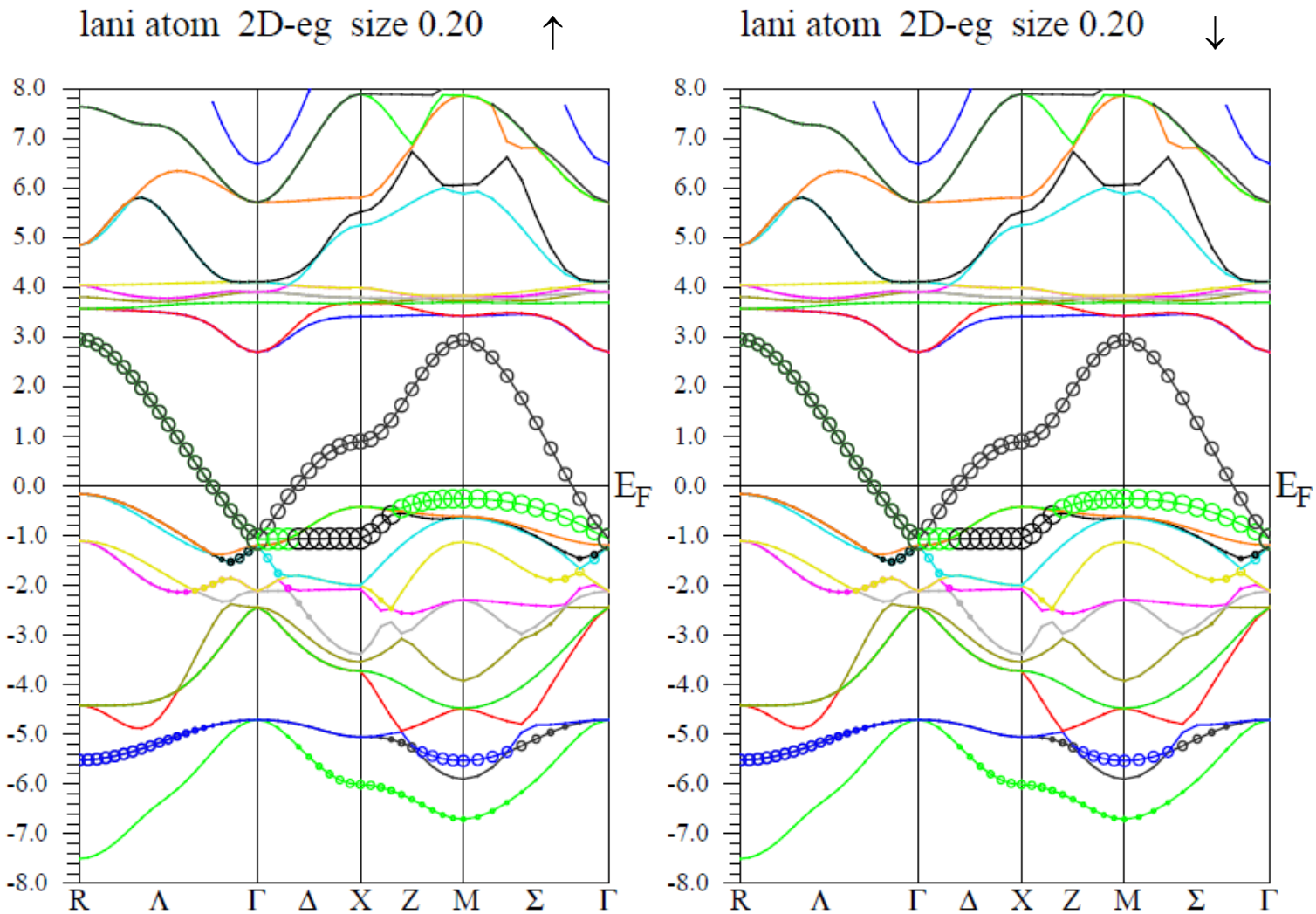


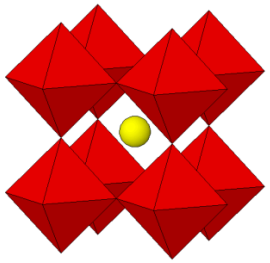

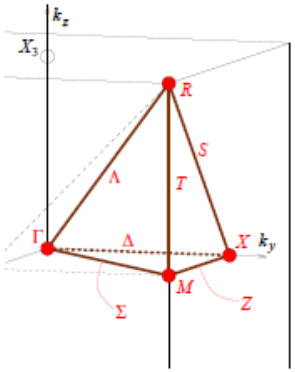


Figure 7: $LaNiO_3$, $d^7 - t_{2g}^6 e_g^1$, Ni-$e_g$

# $LaNiO_3$ – Ni-$d^7$ : oxygen bands

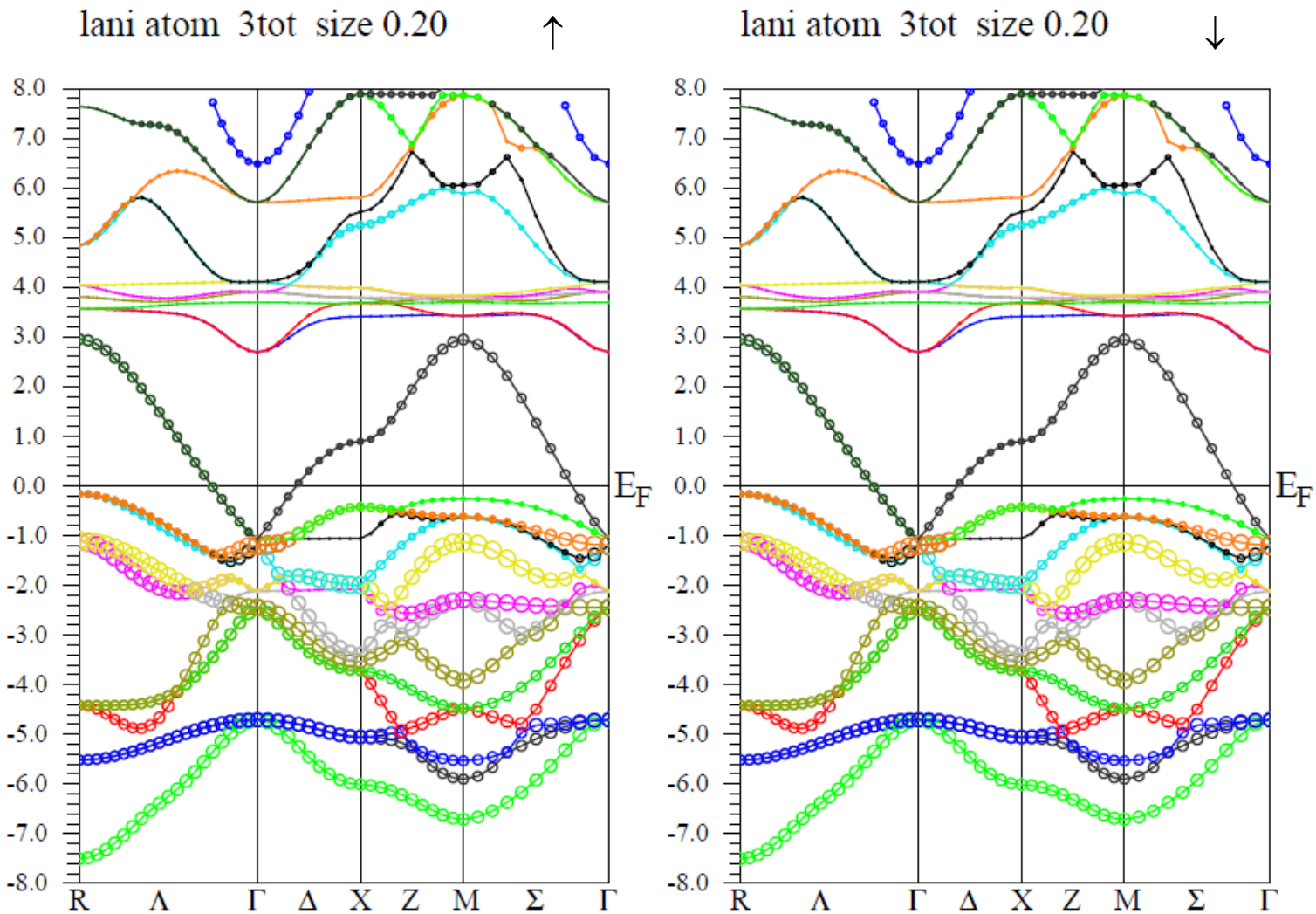


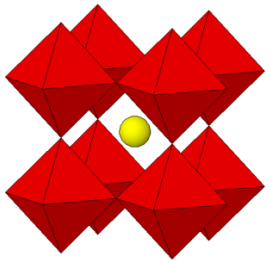

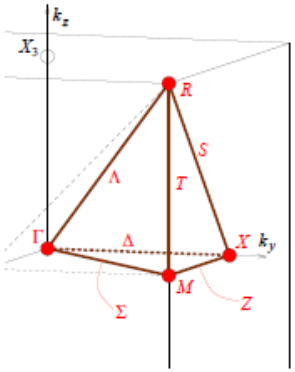


Figure 8: $LaNiO_3$, $d^7 - t_{2g}^6 e_g^1$, O

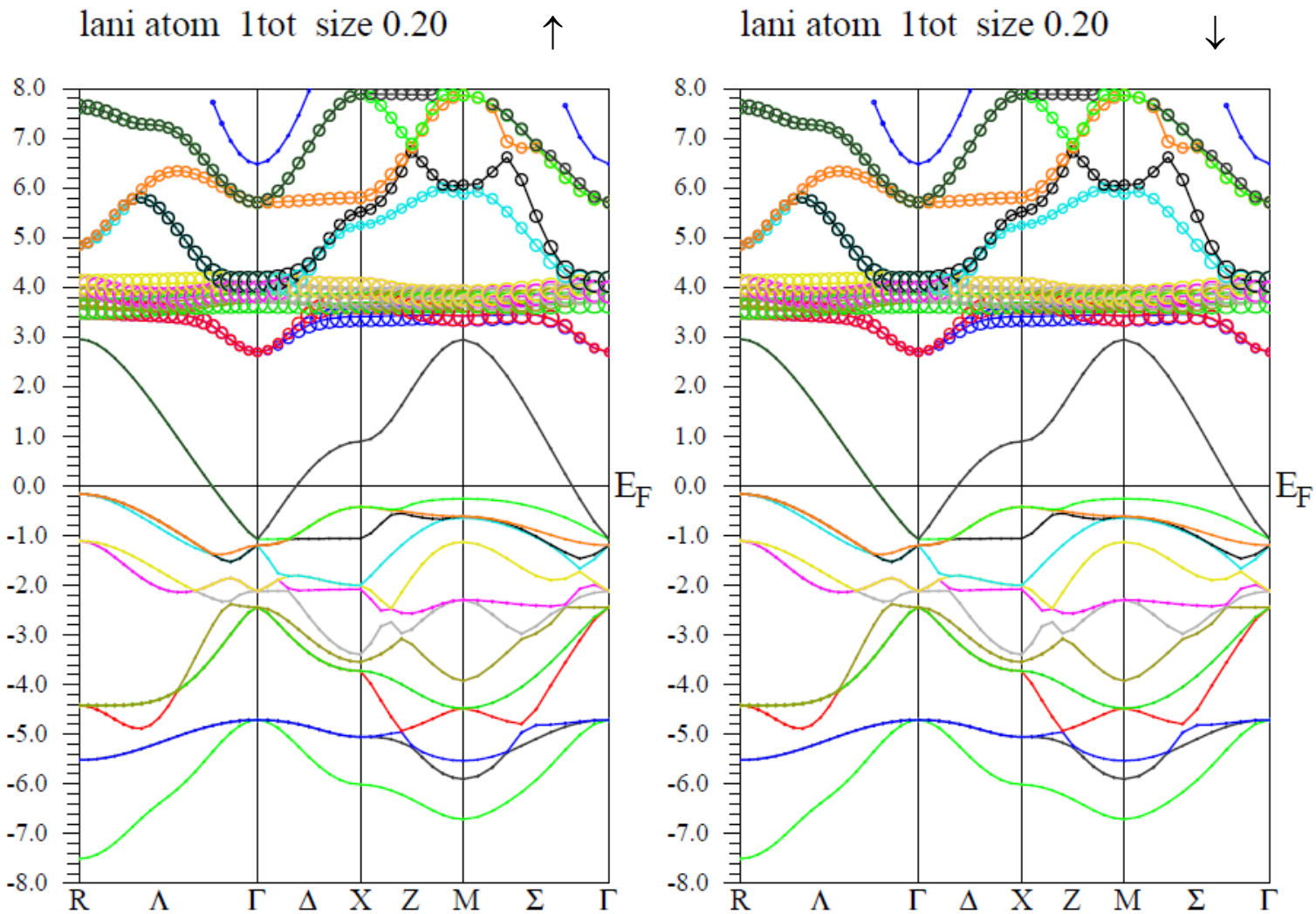


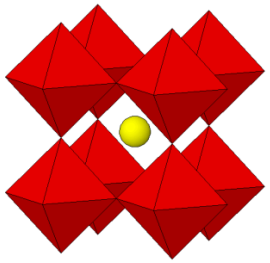

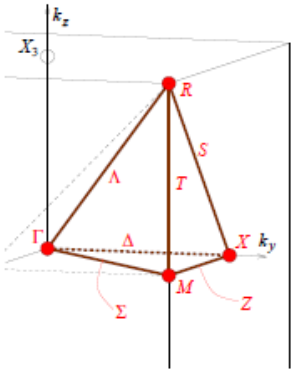


Figure 9: $LaNiO_3$, $d^7 - t_{2g}^6 e_g^1$, La

ZnS - sphalerite

Zn: $d^{10}$ – $t_{2g}^{6}e_{g}^{4}$

F43m

tetrahedra

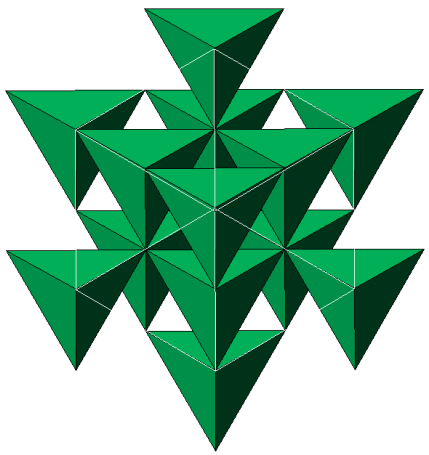

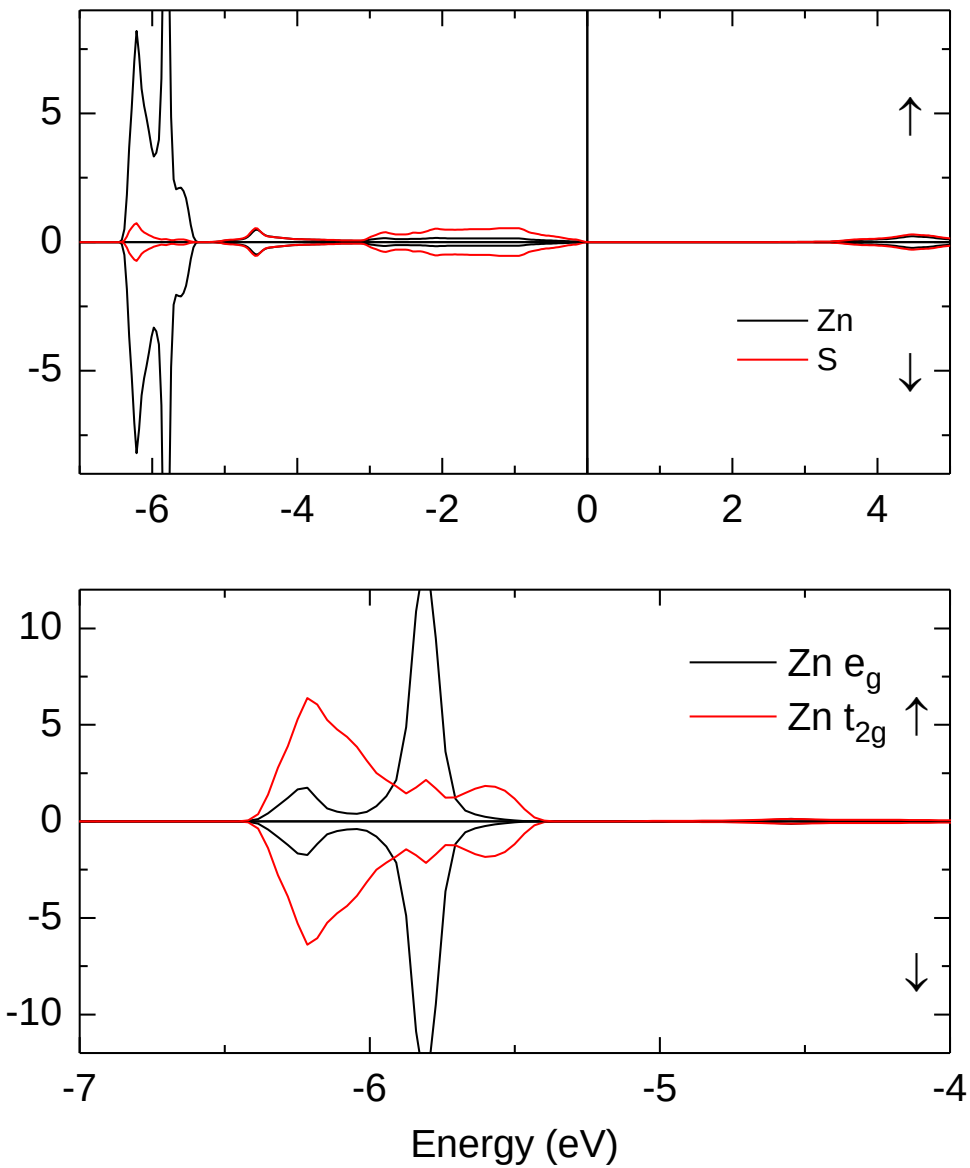

ZnS - wurtzite

Zn: $d^{10}$ – trigonal splitting

$P6_3mc$

tetrahedra

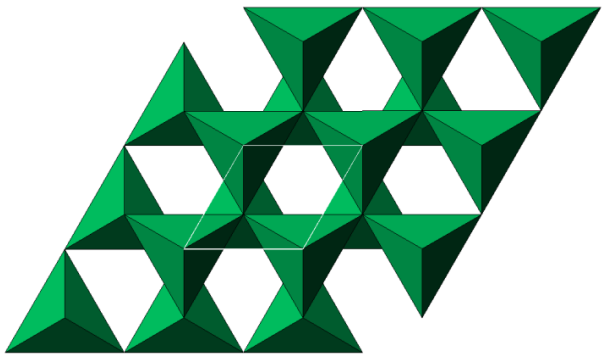

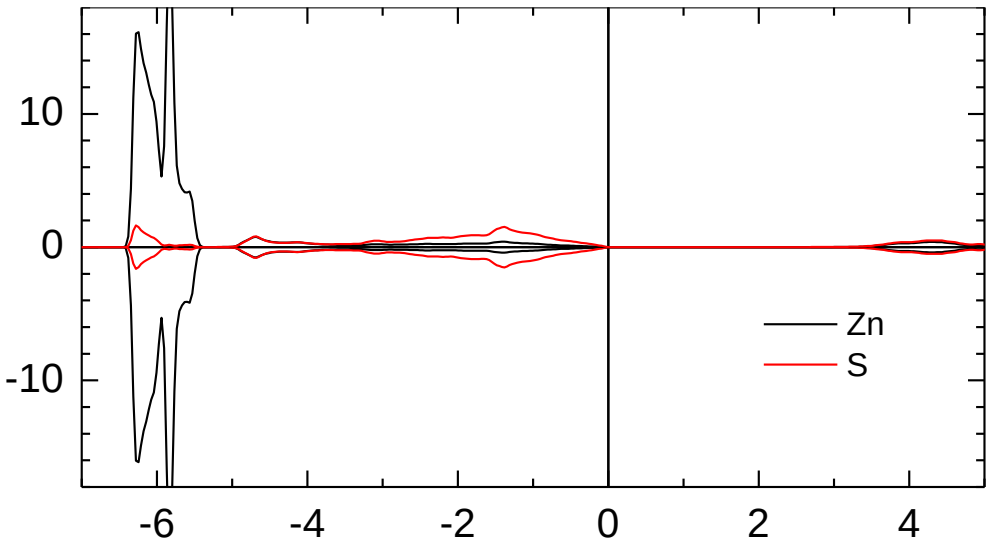


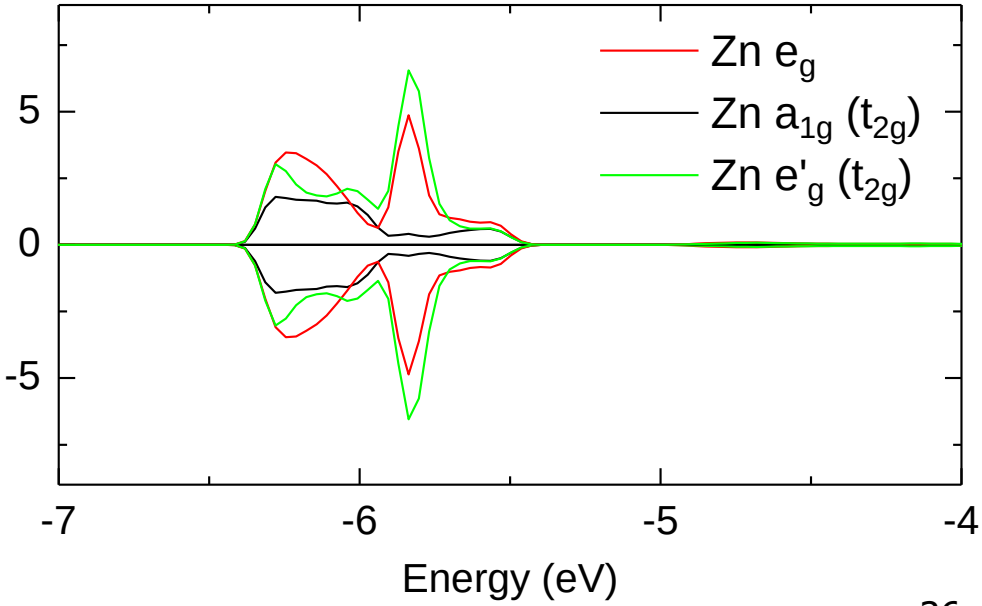

# Trigonally distorted octahedra

Trigonally distorted octahedral: $t_{2g}$ orbitals splits further to $a_{1g}$ and $e'_g$.

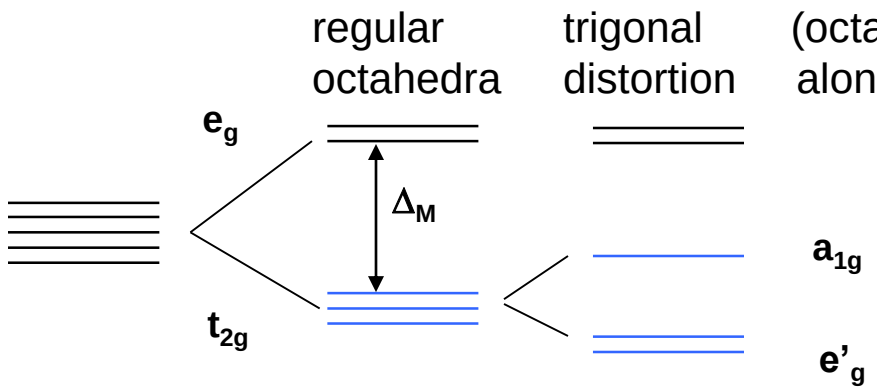


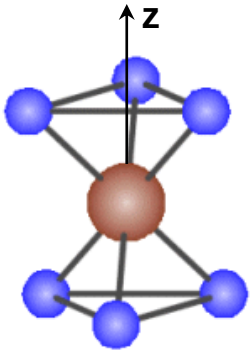


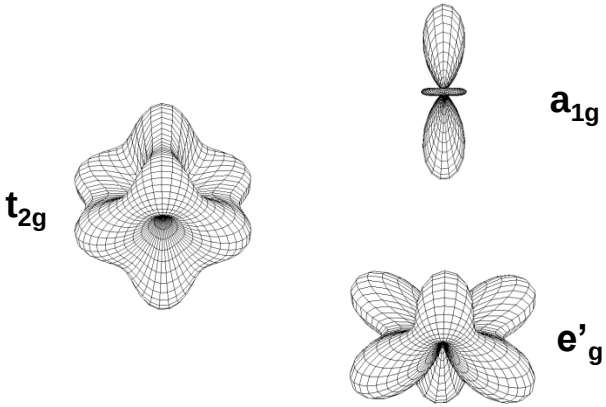


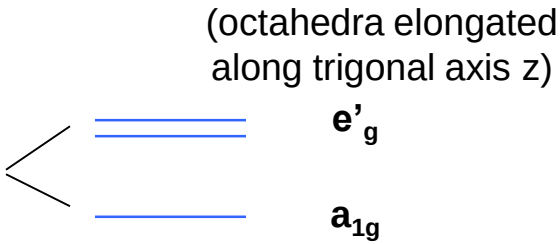

$CdCl_2$

Cd: $d^{10}$ – trigonal splitting

R3m

Edge sharing octahedra

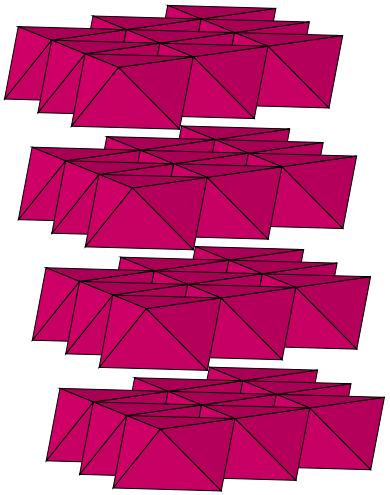

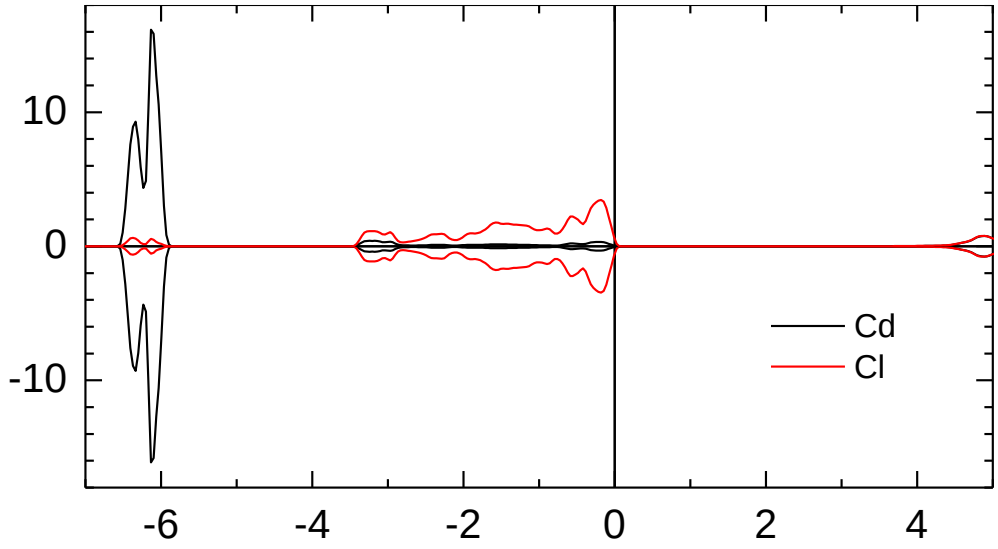


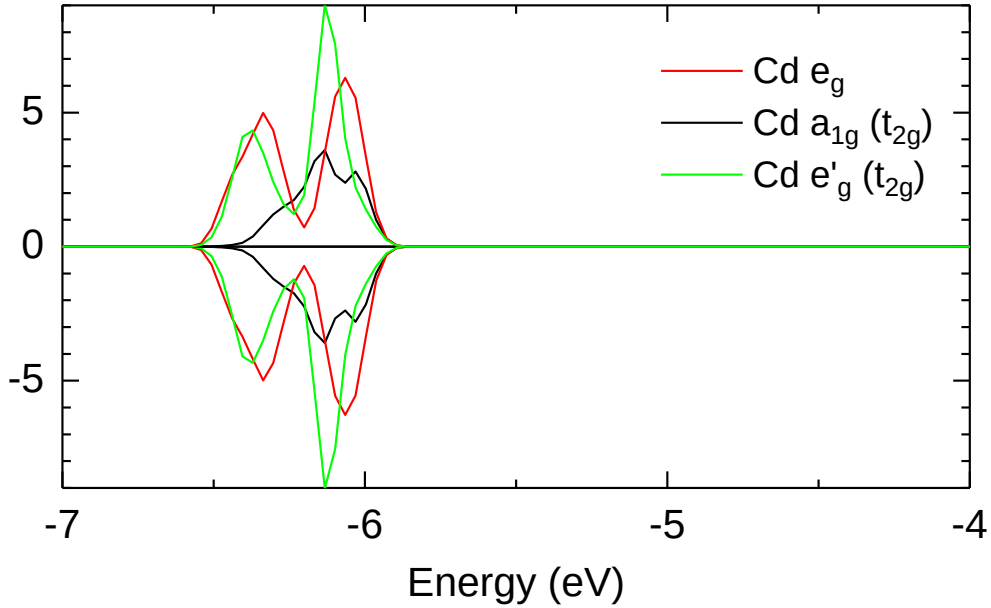

# $Na_xCoO_2$ (x=0.9)

DFT

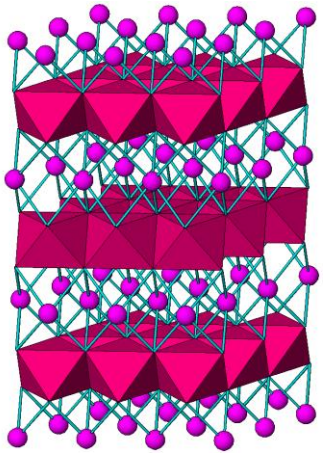

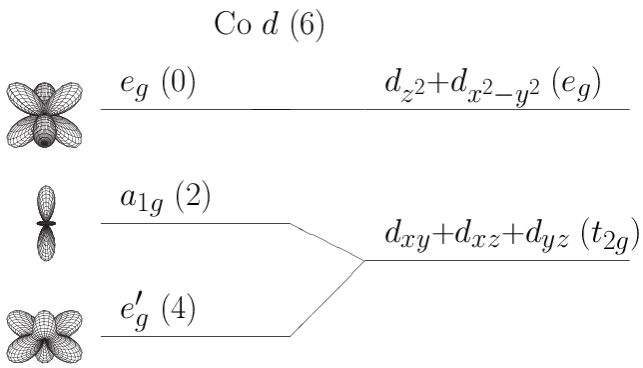


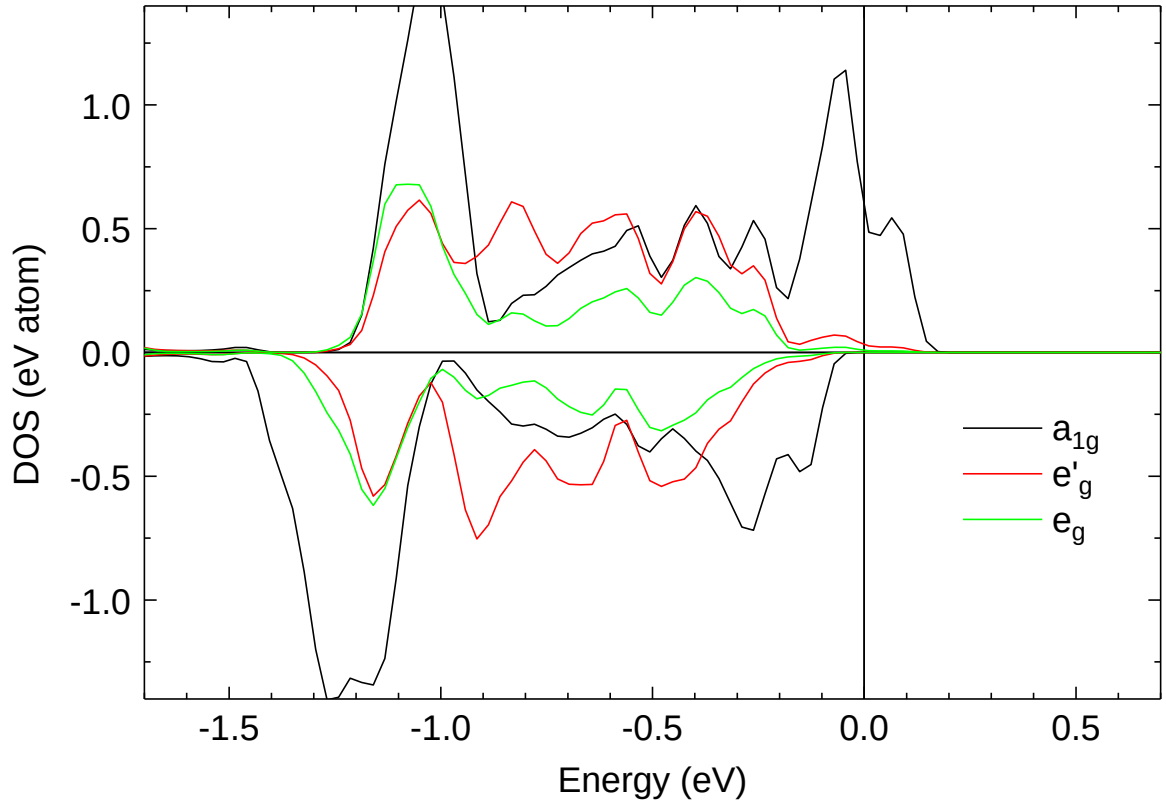

# $CuCoO_2$ delafosite

DFT

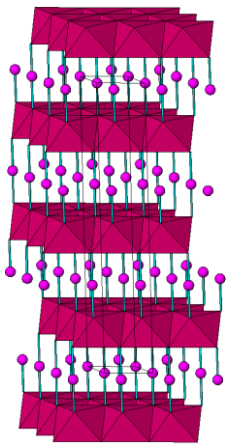

$CoO_6$ trigonal deformation of octahedra
Cu in linear coordination

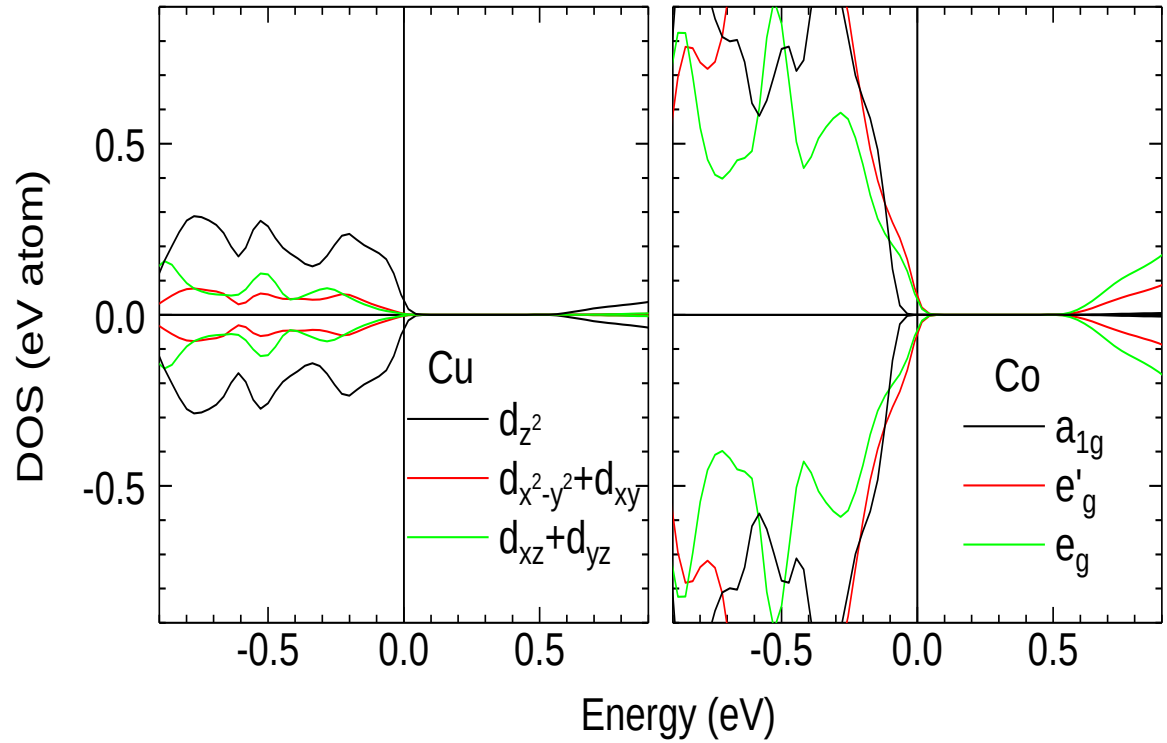


hybridization Co-$a_{1g}$ and Cu-$d_{z^2}$.

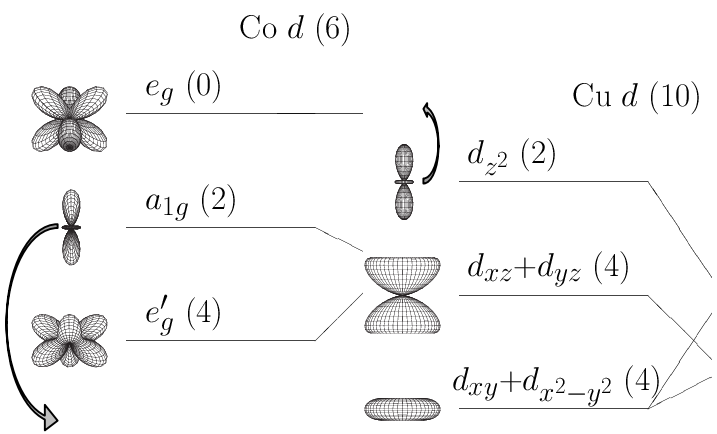


The band structure of $CuCoO_2$ is influenced by the hybridization between symmetrically related Co-$a_{1g}$ and Cu-$d_z^2$ orbitals, which pushes the Co-$a_{1g}$ orbital down below the Fermi level, so that bands at $E_F$ have the Co-$e_g$' and $e_g$ character.

This is in contrast to the band structure of thermoelectric material $Na_xCoO_2$, where the band crossing Fermi level has the $a_{1g}$ character, in accordance with one-electron levels splitting in the crystal field of trigonal coordination compressed along the *z-axis.*